

On the drive of $n\phi = 0$ modes by ICRF accelerated ions in a tokamak



Citation for the original published paper (version of record):

Eriksson, L., Porcelli, F. (2025). On the drive of $n\phi = 0$ modes by ICRF accelerated ions in a tokamak. Nuclear Fusion, 65(9). http://dx.doi.org/10.1088/1741-4326/adf79e

N.B. When citing this work, cite the original published paper.

research.chalmers.se offers the possibility of retrieving research publications produced at Chalmers University of Technology. It covers all kind of research output: articles, dissertations, conference papers, reports etc. since 2004. research.chalmers.se is administrated and maintained by Chalmers Library



PAPER • OPEN ACCESS

On the drive of $n_{\phi} = 0$ modes by ICRF accelerated ions in a tokamak

To cite this article: L.-G. Eriksson and F. Porcelli 2025 Nucl. Fusion 65 092005

View the <u>article online</u> for updates and enhancements.

You may also like

- Fatigue lifetime prediction and reliability assessment for fusion blankets under pulsed operational loading Qingzhu Liang, Xuebin Ma, Xiaoman Cheng et al.
- CXRS measurements of energetic helium ions in ASDEX Upgrade plasmas heated with a 3-ion ICRF scenario A. Kappatou, M. Weiland, R. Bilato et al.
- Velocity space resolved absolute measurement of fast ion losses induced by a tearing mode in the ASDEX Upgrade tokamak
- J. Galdon-Quiroga, M. Garcia-Munoz, L. Sanchis-Sanchez et al.

Nucl. Fusion 65 (2025) 092005 (23pp)

https://doi.org/10.1088/1741-4326/adf79e

On the drive of $n_{\phi}=0$ modes by ICRF accelerated ions in a tokamak

L.-G. Eriksson^{1,*} and F. Porcelli²

- Department of Space, Earth and Environment, Chalmers University of Technology, Gothenburg SE-412 96, Sweden
- ² Department of Applied Science and Technology, Polytechnic University of Turin, Torino 10129, Italy

E-mail: larsgore@chalmers.se

Received 14 April 2025, revised 31 July 2025 Accepted for publication 4 August 2025 Published 14 August 2025



Abstract

Energetic ions have the potential to drive instabilities with toroidal mode number $n_\phi=0$ in tokamak fusion plasmas. A necessary condition is that their distribution function is either anisotropic or exhibits a region of phase space with a positive slope in the energy direction (so-called 'bump-on-tail' distribution). Here an exploration of both possibilities is presented for Ion Cyclotron Range of Frequency (ICRF) accelerated energetic ions. It is found that ion cyclotron resonance layers placed on the high-field side of the magnetic axis provide the most conducive conditions for the drive of vertical $n_\phi=0$ modes. We also discuss to what extent sawtooth redistribution of the ICRF accelerated ions can transiently lead to distribution functions that are locally inverted in the energy direction. However, the latter effect appears to be less efficient in driving $n_\phi=0$ vertical modes than velocity space anisotropy for high-field-side resonances.

Keywords: tokamak, axisymmetric modes, ion cyclotron resonance frequency accelerated ions

(Some figures may appear in colour only in the online journal)

1. Introduction

Auxiliary heating of tokamak plasma by waves in the Ion Cyclotron Range of Frequencies (ICRFs) has proven to be effective and has the potential to provide ion heating in reactor grade plasmas [1, 2]. A characteristic of high power ICRF heating in present day tokamaks is the generation of anisotropic high energy tails on the distribution functions of the resonating ions [3]. Such tails can drive fast ion instabilities, which are routinely observed in experiments, see, e.g. [4, 5] and other references cited therein.

* Author to whom any correspondence should be addressed.

Original Content from this work may be used under the terms of the Creative Commons Attribution 4.0 licence. Any further distribution of this work must maintain attribution to the author(s) and the title of the work, journal citation and DOI.

The mode number spectrum of fast-ion-driven instabilities is intimately linked to the phase-space distribution of the resonating ions. A special case is presented by axisymmetric modes, that is, modes with toroidal mode number equal to zero $(n_{\phi}=0)$. For such modes to be driven by energetic ions, a necessary condition is that their energy distribution be locally inverted in the energy direction (i.e. the derivative of the distribution function in the energy direction of phase space must be positive), or be strongly anisotropic in velocity space. In the current article, we examine both possibilities.

There are four different types of $n_{\phi}=0$ modes in tokamaks. The first type is axisymmetric vertical displacements. These are zero-frequency modes, which grow on the relatively slow resistive wall time scale (under conditions of passive wall stabilisation), and which are normally suppressed by active feedback stabilisation. If left uncontrolled, these modes would cause a vertical displacement event and undesirable disruption of the tokamak discharge [6, 7]. The second type is Geodesic Acoustic Modes (GAMs) [8]. These are

modes that oscillate with a frequency close to the sound frequency. The third and fourth types are, respectively, Global Alfvén Eigenmodes (GAEs) [9] and Vertical Displacement Oscillatory Modes (VDOMs) [10], which both oscillate with a frequency close to the Alfvén frequency based on the poloidal magnetic field. The main point of distinction between GAE and VDOM is that, while the GAE is an internal plasma mode whose frequency of oscillation and spatial structure are sensitive to details of the safety factor *q* and plasma density profiles, the VDOM frequency depends on the elliptical elongation of the plasma cross section and on the plasma-wall distance, but is rather insensitive to details of the *q* profile. Also, the VDOM has a global spatial structure corresponding to a nearly rigid vertical shift of the plasma core, with a return flow localised near the plasma edge.

The three finite-frequency modes, GAM, GAE and VDOM, can all be driven unstable by fast ions, provided their distribution functions in velocity space possess special features, as discussed e.g. in [11–14] and also alluded to in the second paragraph of this introduction. We point out that $n_{\phi}=0$ modes have been observed on DIII-D [15] and on JET tokamak experiments [12, 13, 16]. The main purpose of the present article is to investigate whether these special features can develop for minority ions accelerated by ICRF heating. As a case study, we shall focus on VDOM, although many of the results obtained here can be applied also to GAM and GAE.

ICRF accelerates resonating ions mainly in the perpendicular direction and during high power heating they can reach energies in the multi MeV range. Furthermore, pitch angle scattering due to collisions decreases with energy. Consequently, strongly energetic and anisotropic tails tend to develop on the distribution functions of resonating species during high power ICRF heating. Regarding $n_{\phi} = 0$ modes driven unstable by 'bump-on-tail' distributions, the generation of a distribution function with region of a locally positive energy derivative is not trivial. However, a few mechanisms exist. Recent examples are alpha particles generated in DT reactions where their source rate is modulated by sawteeth oscillations in the centre of the plasma [17] and NBI injection with modulated power [15]. In the case of fast ions generated by ICRF heating, it is harder to generate energy inverted distributions because the acceleration of the resonating particles is governed by a diffusive process in velocity space [3]. A characteristic of diffusion is that it tries to smooth out the energy distribution. For instance, a modulation of the ICRF power only leads to a modulation of the averaged energy of the resonating ions without affecting the monotonic decrease of their distribution with energy. On the other hand, there is evidence that MHD activity can lead to locally energy inverted distributions of ICRF accelerated ions [18]. Another possibility is presented by the redistribution of fast ions during a sawtooth crash because if, as has been argued [19], fast trapped ions are less redistributed than lower energy ones, it is possible to create an inverted energy distribution in the centre of the plasma. An exploratory study of this mechanism in presented in the current paper. More specifically, we examine the period during which such an inverted distribution is maintained. This period turns out to be relatively short because the ICRF-induced velocity space diffusion tries to restore a monotonic distribution function. Furthermore, there is no sharp dividing line in energy between ions that are redistributed and those that are not [20] and the energy around which the transition takes place scales with the sawtooth crash time [19]. The influence of these factors on the potential for creating distribution functions inverted in the energy direction is investigated in this article.

In order to investigate the potential drive of vertical $n_\phi=0$ modes by ICRF-accelerated ions, two approaches have been employed. First, a semi-analytical procedure, using a model distribution function, has been utilised to shed light on the key factors for the drive of the $n_\phi=0$ mode through the anisotropy of the distribution function. Secondly, numerical simulations of the distribution of the resonating ions have been performed and used as input to a code that analyses the linear stability criterion for the $n_\phi=0$ modes. The drive for the $n_\phi=0$ mode through the anisotropy of the distribution function, and for locally inverted energy distribution following a sawtooth crash, has been assessed in these numerical simulations.

2. Necessary conditions for fast ion driven modes

The $n_{\phi}=0$ VDOM modes of interest in the current work are characterised by $\omega_0<<\omega_{\rm c}$, where ω_0 is the real part of the instability angular frequency and $\omega_{\rm c}$ is the ion cyclotron angular frequency. Resonant wave particle interaction, implying exchange of energy, with a low frequency instability, takes place when a global resonance condition,

$$\omega_0 = p\omega_b + n_\phi \langle \dot{\phi} \rangle \tag{1}$$

is fulfilled. Here ω_b is the bounce/transit frequency of a particle (note that we use the same notation, i.e. ω_b , for the bounce frequency of trapped particles and for the transit frequency of passing ones), $\langle \dot{\phi} \rangle$ is its toroidal precession frequency, and p is an integer (typically a small number). The physical meaning of this resonance condition is simply that a particle on an unperturbed orbit feels the same wave phase after one revolution of the orbit (otherwise changes of the energy would not accumulate in the linear phase).

The distribution function, f_0 , of energetic ions on time scales much longer than the bounce time can be characterised by three invaraints of the unperturbed motion, see e.g. [21]: the particle kinetic energy \mathcal{E} ; a generalised pitch angle variable, $\Lambda = \mu B_0/\mathcal{E}$, where μ is the magnetic moment; and the toroidal angular momentum $P_\phi = mRv_\parallel B_\phi/B + Ze\psi$, where ψ is the poloidal flux function; it is also necessary to introduce a variable σ that takes the value -1 and 1 depending on the sign of v_\parallel at the minimum magnetic field point along an orbit (to separate ions on co- and counter-current passing orbits). During resonant interaction, the changes in energy, Λ , and P_ϕ are related through: $\Delta\Lambda = -(\Lambda/\mathcal{E})\Delta\mathcal{E}$ and $\Delta P_\phi = (n_\phi/\omega)\Delta\mathcal{E}$, see e.g. [22] (the latter also follows from a quantum mechanical consideration: a resonant particle either emitting or

absorbing a wave quantum receives a change of its energy $\Delta \mathcal{E} = \pm \hbar \omega$, while its toroidal angular momentum changes by an amount $\Delta P_{\phi} = \pm R k_{\phi} \hbar = \pm n_{\phi} \hbar$, therefore $\Delta P_{\phi}/\Delta \mathcal{E} = n_{\phi}/\omega$; the expression for the change in Λ is simply a consequence of the magnetic momentum remaining constant in the presence of low frequency modes). Thus, the resonant wave particle interaction implies a 'kick path' in phase space. Assuming that the wave particle phase is random and there are more particles at the higher energy end of this path than at the lower end, there will be a finite transfer of energy from the particles to the wave instability. Therefore, we can write the necessary condition for an instability as

$$\frac{\partial f_0}{\partial \mathcal{E}} + \frac{\partial f_0}{\partial \Lambda} \frac{\partial \Lambda}{\partial \mathcal{E}} + \frac{\partial f_0}{\partial P_{\phi}} \frac{\partial P_{\phi}}{\partial \mathcal{E}} = \frac{\partial f_0}{\partial \mathcal{E}} - \frac{\Lambda}{\mathcal{E}} \frac{\partial f_0}{\partial \Lambda} + \frac{n_{\phi}}{\omega_0} \frac{\partial f_0}{\partial P_{\phi}} > 0, \tag{2}$$

where $f_0 = f_0(\mathcal{E}, \Lambda, P_{\phi}, t)$.

Equation (2) can be seen as a generalisation of the standard 'bump on tail' argument for instability drive. Loosely speaking, the criterion depends on the direction of the tail in phase space (i.e. the direction of the kick path). For finite toroidal mode numbers n_{ϕ} , instabilities can be driven by gradients in P_{ϕ} , and because trapped fast ions have $P_{\phi} = Ze\psi_{\rm t.p.}$, where 't.p.' stands for turning point, one can see that gradients in P_{ϕ} are linked to pressure gradients of the fast ions. On the other hand, for $n_{\phi} = 0$ modes, only gradients in \mathcal{E} and Λ come into play.

Here it should be remarked that in this work a region with a pure energy inverted distribution is taken to mean,

$$\left. \frac{\partial f_0}{\partial \mathcal{E}} \right|_{\Lambda = const.} > 0.$$
 (3)

This is in contrast to [12], where an energy inverted distribution function is discussed in the context of,

$$\frac{\partial f_0}{\partial \mathcal{E}}\Big|_{u=const} > 0.$$
 (4)

When analysing the anisotropy of the distribution function, the first choice is more natural (μ and \mathcal{E} are far from being orthogonal, especially for ICRF accelerated ions that are accelerated mainly in the perpendicular direction).

Regions of phase space where equations (1) and (2) are fulfilled are necessary conditions for instability. However, they are not sufficient because other regions in phase space, as well as core plasma dissipation or wall resistivity (the latter being relevant for the VDOM case) can provide damping, giving rise to instability thresholds. More details on the instability criterion are presented in the next section.

3. Linear theory of $n_\phi=0$ modes driven by energetic ions

In this section we present a very brief summary of the linear theory of $n_{\phi}=0$ modes driven unstable by fast ions. For more details, the reader is referred to [10, 14] and appendix A. The

relevant dispersion relation for the complex mode frequency ω can be written as

$$\omega^2 = \omega_0^2 - 2i\omega_0\gamma_\eta + i\omega_0^2\lambda_h + \mathcal{O}\left(\gamma^2/\omega_0^2\right),\tag{5}$$

where ω_0 is a real quantity approximately equal to the $n_\phi=0$ oscillation frequency, γ_η is the damping rate due to various mechanisms (such as core plasma dissipation and wall resistivity), and λ_h is a dimensionless parameter representing the non-adiabatic part of the normalised energy functional, $\mathrm{Im}(\delta \hat{W}_{h,\mathrm{nad}})$, of the energetic ions, as defined, e.g. in [23]. Assuming $\gamma_{\mathrm{tot}} \ll \omega_0$, the imaginary part of the mode frequency ω then takes the form $\gamma_{\mathrm{tot}} = \omega_0 \lambda_h/2 - \gamma_\eta$. The threshold condition for instability is

$$\lambda_h \geqslant \frac{2\gamma_\eta}{\omega_0}.$$
 (6)

In [14], it was shown that λ_h is proportional to the fast particle density, n_h , and that, for realistic values of γ_η , instability requires ratios of fast particle to core plasma density ranging between 10^{-3} and 10^{-2} . However, the sign and value of the constant of proportionality between λ_h and n_h depends on details of the fast ion distribution, as explained in the discussion that follows.

By definition we have,

$$\lambda_h = \frac{-2}{\omega_0 W_{\text{inst}}} \frac{\mathrm{d}W_h}{\mathrm{d}t},\tag{7}$$

where W_h is the energy content of the energetic ions, and the kinetic energy associated with the instability is taken to be

$$W_{\rm inst} = \frac{1}{2} \rho_c \omega_0^2 \xi^2, \tag{8}$$

 ρ_c is the mass density of the plasma and $\xi = |\vec{\xi}|$ represents the magnitude of the displacement vector $\vec{\xi}$ of a field line. In order to connect with the notation frequently found in the literature and used in [14], one should note that $\omega_0 \mathrm{Im}(\delta W_{h,\mathrm{nad}})/2 = \mathrm{d}W_h/\mathrm{d}t$. The expression for λ_h can be obtained from a straightforward generalisation of equation (11) in [14]. However, for completeness, a brief alternative derivation is presented in appendix A, where $\mathrm{d}W_h/\mathrm{d}t$ is calculated starting from quasilinear theory.

In the thin banana width limit one finds,

$$\lambda_{h} = \zeta \sum_{\sigma} \int \left[\sum_{p} \frac{|\Upsilon_{p}|^{2}}{h_{\omega_{b}}} \mathcal{E}^{3/2} \left(\frac{\partial f_{0}}{\partial \mathcal{E}} - \frac{\Lambda}{\mathcal{E}} \frac{\partial f_{0}}{\partial \Lambda} \right) \right]_{\mathcal{E} = \mathcal{E}_{p}^{*}} \rho d\rho d\Lambda$$
$$= \sum_{p} \int \lambda'_{h,p} (\rho) d\rho \tag{9}$$

where $\lambda'_{h,p}(\rho)$ is the contribution from a given flux surface, and the summation is over the harmonics of the orbit periodicity at equilibrium. The flux surface label is defined as,

$$\rho = \sqrt{\psi/\psi_a},\tag{10}$$

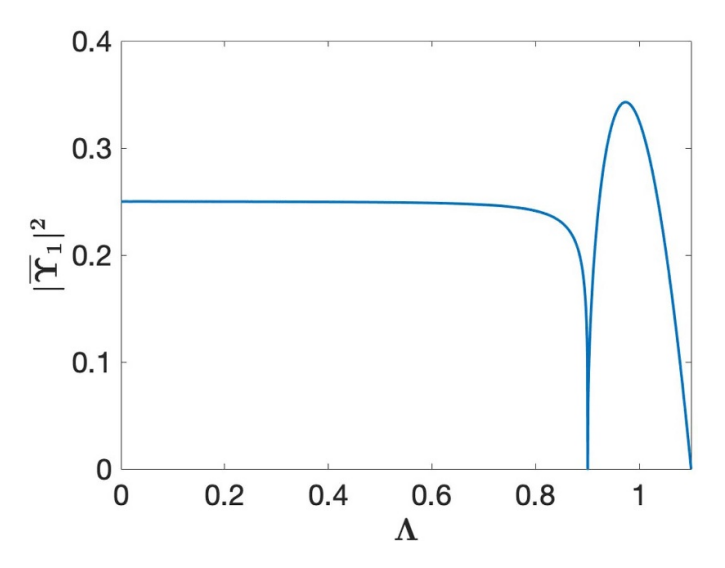


Figure 1. Illustration $|\overline{\Upsilon}_1|^2$ for typical case, with circular flux surfaces and r/R = 0.1.

 ψ is the poloidal flux function here defined to be zero on the magnetic axis, ψ_a is the value of ψ at the plasma boundary. Following [14], the normalisation constant ζ is defined by

$$\zeta = \frac{16\sqrt{2}\pi^4 R_0 q \psi_a}{V \rho_c \omega_0^2 \xi^2 B_0 m^{3/2}},\tag{11}$$

and we have introduced the function $h_{\omega_b}(\Lambda,\rho) = \omega_b R_0 q/v$ (valid in the thin banana width limit). For a given Λ and ρ , the resonant energy \mathcal{E}_p^* is defined by the resonance condition for ions interacting with $n_{\phi} = 0$ modes,

$$\omega_0 = p\omega_b\left(\mathcal{E}_p^*, \Lambda, \rho\right). \tag{12}$$

Thus,

$$\mathcal{E}_{p}^{*}\left(\omega_{0},\Lambda,\rho\right) = \frac{m}{2} \left[\frac{\omega_{0} R_{0} q}{p h_{\omega_{b}}\left(\Lambda,\rho\right)} \right]^{2}.$$
 (13)

Furthermore, $|\Upsilon_p|$, is the modulo of the Fourier-decomposed, complex perturbed Hamiltonian, H_1 , which is derived in appendix A and given by,

$$\begin{aligned} |\Upsilon_{p}| &= \left| \frac{1}{\tau_{b}} \int_{0}^{\tau_{b}} \mathcal{E}\left(2 - \Lambda \frac{B}{B_{0}}\right) \vec{\xi} \cdot \vec{\kappa} \, \mathrm{e}^{-\mathrm{i}p\omega_{b}\tau} \mathrm{d}\tau \right| \\ &\approx \left| \frac{1}{\tau_{b}} \int_{0}^{\tau_{b}} \mathcal{E}\left(2 - \Lambda\right) \vec{\xi} \cdot \vec{\kappa} \, \mathrm{e}^{-\mathrm{i}p\omega_{b}\tau} \mathrm{d}\tau \right|, \end{aligned} \tag{14}$$

where $\mathrm{d}\tau$ is the bounce time differential and $\vec{\kappa}$ is the magnetic curvature vector. The physics behind the perturbation of the particle Hamiltonian reflected in Υ_p is the force of the perturbed electric field in the drift direction, $H_1 \sim \vec{E_1} \cdot \vec{v_D}$, of a resonating ion. In order to establish contact with [14], we note that in perturbation theory the perturbed Lagrangian, L_1 is just the negative of the perturbed Hamiltonian, see e.g. [23], i.e. $|L_1| = |H_1|$.

The analysis up to equation (14) is valid for all three types of $n_{\phi} = 0$ modes mentioned in the Introduction, i.e. GAM, GAE, and VDOM. Now, we specialise to the case of VDOM.

Because in this case plasma displacements are along the vertical direction, the curvature related to the toroidal magnetic field component will not contribute to the scalar product $\vec{\kappa} \cdot \vec{\xi}$. Instead, it is the curvature of the poloidal field component that plays the key role for VDOM. One finds approximately

$$\vec{\xi} \cdot \vec{\kappa} \approx \frac{\xi_0}{B} \frac{\partial B_{\theta}}{\partial \rho} \hat{z} \cdot \nabla \rho, \tag{15}$$

where ξ_0 is the amplitude of the vertical displacement on the magnetic axis. For a tokamak equilibrium such that the cross sections of the flux surfaces can be approximated by concentric circles, this expression up to corrections of the order of the local inverse aspect ratio $\epsilon = r/R_0$ is given by,

$$\vec{\xi} \cdot \vec{\kappa} \approx \frac{\epsilon^2 \xi_0}{q^2 r} \sin(\theta). \tag{16}$$

In what follows, we will also use a normalised form of Υ_p ,

$$\overline{\Upsilon}_p = \frac{\Upsilon_p}{\mathcal{E}\sqrt{h_{\omega_b}}\xi_0} \tag{17}$$

The dominant term corresponds to p = 1. The quantity $|\overline{\Upsilon}_1|^2$ as function of Λ is shown if figure 1 for parameter values that are typical of a tokamak equilibrium.

One should note that $\xi \cdot \vec{\kappa}$ is an odd function of θ and therefore only the $\sin(p\omega_b\tau)$ part of the exponential in equation (14) can contribute to the integral in an up-down symmetric plasma. Furthermore, for p=2 we have, $\sin(p\omega_b\tau)=0$ at the turning point of a trapped particle. For reasons of symmetry, the integration appearing in equation (14) along the outer leg of a trapped orbit is then cancelled by the integration along the inner leg in the thin banana width limit. Thus, for an up-down symmetric plasma and in the thin banana width limit $\overline{\Upsilon}_p$ vanishes in the trapped particle region for even values of p. This corrects an erroneous statement made in [14], which attributed a nonzero value of $\overline{\Upsilon}_2$ in the trapped particle region. Furthermore, we have verified that the harmonics of $\overline{\Upsilon}_p$ with

 $p \ge 3$ typically have very small values. Therefore, we limit ourselves to values of p = 1 in this work.

Below, we use both a semi-analytical approach and a numerical implementation based on equations (9), (14) and (15) to assess the potential for ICRF accelerated ions driving $n_{\phi} = 0$ modes in the presence of $n_{\phi} = 0$ VDOM.

4. Models and properties of the ICRF accelerated ion distribution function

For the current exploratory study, we adopt a simplified model. The distribution function of the ICRF heated ions is simulated by the PION code [24]. The code adopts a model ICRF wave propagation that was designed to approximate the results of a full wave code [25], and a Fokker-Planck solver for the pitch angle averaged distribution function of a flux surface labelled by ρ , $F(\mathcal{E}, \rho)$, together with a model for the anisotropy of the distribution function [24]. The power deposition and Fokker-Planck calculations in PION are self-consistent in the sense that: (i) an effective parallel temperature of the distribution function is obtained from the Fokker-Planck calculation and used in the wave propagation module to account for the Doppler broadening of the cyclotron resonance; (ii) the absorption strength in the wave propagation code is updated to be consistent with that of the Fokker-Planck module as the resonating ion distribution function evolve in time [26]. In this work we neglect finite orbit width effects.

As outlined above, for the purposes of analysing the potential for the ICRF accelerated ions to drive $n_{\phi}=0$ modes, it is necessary to have an adequate description of the anisotropy of the distribution function of the resonating ions. A key feature of ICRF wave particle interaction is that the change in Λ experienced by a resonating particle as it passes a resonance $\omega_{\rm IC} - \vec{k} \cdot \vec{v_{\rm g}} = n\omega_{\rm ci}$ (where $\omega_{\rm CI}$ is the ICRF wave angular frequency, \vec{k} the wave vector, $v_{\rm g}$ is the guiding centre velocity and $\omega_{\rm ci}$ is the ion cyclotron frequency of the resonating species; the label IC is used throughout to distinguish the ICRF-related quantities from those of the $n_{\phi}=0$ wave) is related to the change in energy as

$$\Delta \Lambda = \frac{n\omega_{\text{ci},0} - \Lambda\omega_{\text{IC}}}{\omega \mathcal{E}} \Delta \mathcal{E}, \tag{18}$$

where $\omega_{ci,0}$ is the cyclotron frequency on the magnetic axis. This expression is derived from the characteristics of the quasilinear operator describing the wave particle interaction (see e.g. [27]). Consequently, as ions resonating with the ICRF wave are accelerated to higher energies, their pitch angle Λ approaches the value

$$\Lambda_{\rm IC} = \frac{n\omega_{\rm ci,0}}{\omega_{\rm IC}}.\tag{19}$$

Collisional pitch angle scattering, on the other hand, will limit the narrowness of the distribution function of the high energy resonating ions around $\Lambda=\Lambda_{IC}.$ The strength of pitch angle scattering diminishes with the energy of a resonating ions, i.e. the width of the distribution function around $\Lambda=\Lambda_{IC}$ decreases with energy. The result is a distribution function,

in the thin banana with limit, with the well known rabbit-ear shape of the level surfaces [28] when expressed in the invariants $(v_{\perp 0}, v_{\parallel 0})$ (the perpendicular and parallel velocities in the mid-plane of a resonating ion). In order to model the anisotropy of the distribution function in PION, we use an updated version of the Fokker–Planck package designed to capture the rabbit-ear-shaped distribution function. The salient features of the extended Fokker–Planck scheme are provided in appendix B. An example of the distribution function obtained with this augmented version of PION is shown in figure 2.

For on-axis resonances, i.e. for $\omega_{\rm IC}=\omega_{\rm ci,0},~\Lambda=\Lambda_{\rm IC}=1$ corresponds to trapped particles with turning points at a magnetic field $B=B_0$, i.e. an almost vertical line through the magnetic axis in a low beta plasma. On the other hand, resonances on the low field side with $\omega_{\rm IC}>n\omega_{\rm ci,0}$ and flux surfaces being close to having $\omega_{\rm IC}=n\omega_{\rm ci}$ in the mid-plane, $\Lambda=\Lambda_{\rm IC}<1$ correspond to ions that are close to the trapped-passing limit. As will be seen below, this will turn out to be important when analysing the drive of $n_\phi=0$ modes by ICRF-accelerated ions.

With the aim of illustrating a few key features of the drive of $n_{\phi} = 0$ modes by anisotropic ICRF accelerated ions, we note that in the high energy range, the distribution function becomes very narrow in the Λ direction, as shown in figure 3.

Consequently, we can adopt an ad-hoc model of the distribution function suitable for a semi-analytical analysis by approximating the Λ dependence at high energy by a delta function. The derivation of such a model for the distribution function is outlined in appendix C, which results in

$$f_0(\mathcal{E}, \Lambda, \rho) \approx F(\mathcal{E}, \rho) \delta(\Lambda - \Lambda_{\rm IC}),$$
 (20)

where

$$F(\mathcal{E}, \rho) = c_F(\rho) \frac{\exp\left(-\frac{\mathcal{E}}{T_{\text{tail}}(\rho)}\right)}{\sqrt{\mathcal{E}}}$$
(21)

and

$$c_F(\rho) = n_h(\rho) \frac{m_h^{3/2} h_{\omega_b}(\Lambda_{\rm IC}, \rho)}{2^{3/2} \pi T_{\rm tail}(\rho)}, \tag{22}$$

where n_h is the density of resonating ions in the tail of the distribution function and m_h their mass. Moreover, this T_{tail} corresponds to the asymptotic perpendicular tail temperature found in [29]. It is important to note that equation (21) is valid only in the region where the distribution function is highly anisotropic, i.e. at energies much greater than thermal.

For a simplified numerical exploration of the effect of the width of the distribution in the Λ direction, on the $n_{\phi}=0$ drive, we will use a version of the above equation with a finite width for the pitch-angle distribution,

$$f_0(\mathcal{E}, \Lambda, \rho) \approx F(\mathcal{E}, \rho) g(\Lambda, \rho)$$
 (23)

where,

$$g(\Lambda, \rho) = C_g \exp \left[-\left(\frac{\Lambda - \Lambda_{\rm IC}}{\Delta \Lambda_{\rm tail}}\right)^2 \right]$$
 (24)

and C_g is a normalisation constant such that equation (B.3) in appendix B is fulfilled.

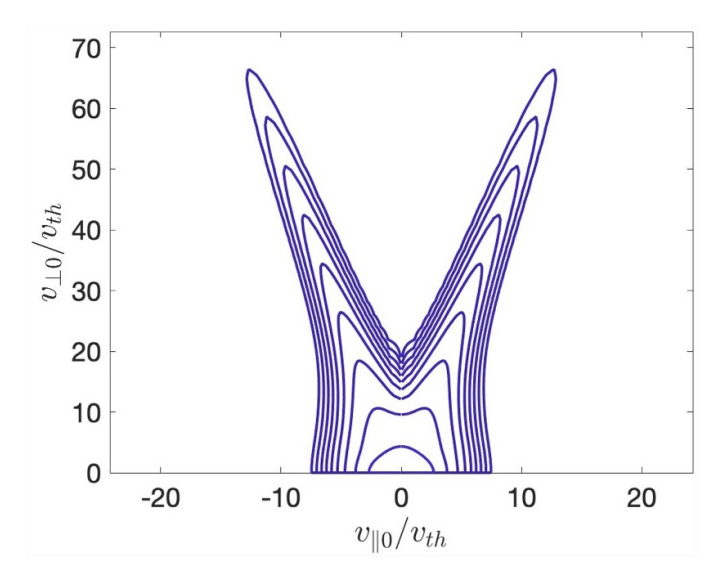


Figure 2. Level surfaces of the simulated distribution function of ICRF accelerated ions for JET like parameters (3 He minority heating in a deuterium plasma, $\omega_{c,^3\text{He}}(B_0) = \omega_{\text{IC}}$, $\rho a/R_0 = 0.04$, $p_{\text{ICRF}} = 3$ MW m $^{-3}$, $n_{\text{e},0} = 3.5 \cdot 10^{19}$, $T_{\text{e}} = T_{\text{i}} = 6$ keV).

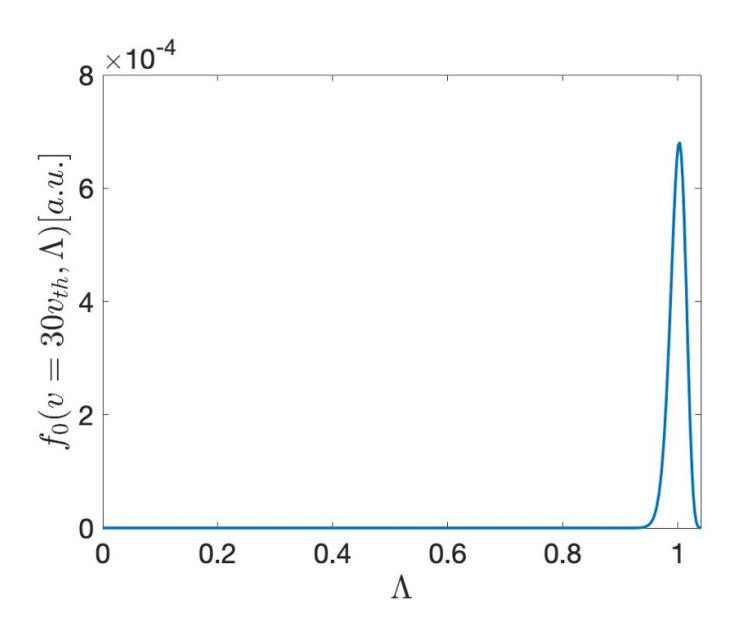


Figure 3. Distribution function at a velocity $v = 30v_{th}$ as a function of Λ for the case in figure 2.

5. Analysis of the $n_\phi=0$ mode drive due to the anisotropy of ICRF accelerated fast ions distribution function

In this section, we first use the simplified model distribution functions discussed above to provide a rudimentary overview of the conditions under which the anisotropy of the distribution of ICRF accelerated ions can drive $n_{\phi}=0$ modes for p=1. The output of the PION simulations is then used as input to equation (9) in a fully numerical calculation of $\lambda_{h,1}$ for a more realistic evaluation of the $n_{\phi}=0$ drive. For illustrative purposes, the $n_{\phi}=0$ mode frequency is scanned up to values of the order of 300 kHz, keeping in mind that the

realistic frequency range for both VDOM and GAE modes in present-day tokamak experiments such as JET is between 100 kHz and 400 kHz.

In order to get insight into factors that are key for the drive of $n_{\phi}=0$ modes, it is instructive to first consider the model of the high-energy distribution with a finite width in Λ centred around $\Lambda_{\rm IC}$. It is evident from equation (9) (where only the term with p=1 is important see our discussion in section 3) that, unless there are regions in phase space where $\partial F/\partial \mathcal{E}$ is positive, only the term involving $\partial f_0/\partial \Lambda$ can contribute to a possible drive of $n_{\phi}=0$ modes. Moreover, only the part of the distribution with $\Lambda>\Lambda_{\rm IC}$ results in a positive contribution to the mode growth rate, while particles with $\Lambda<\Lambda_{\rm IC}$ give rise to

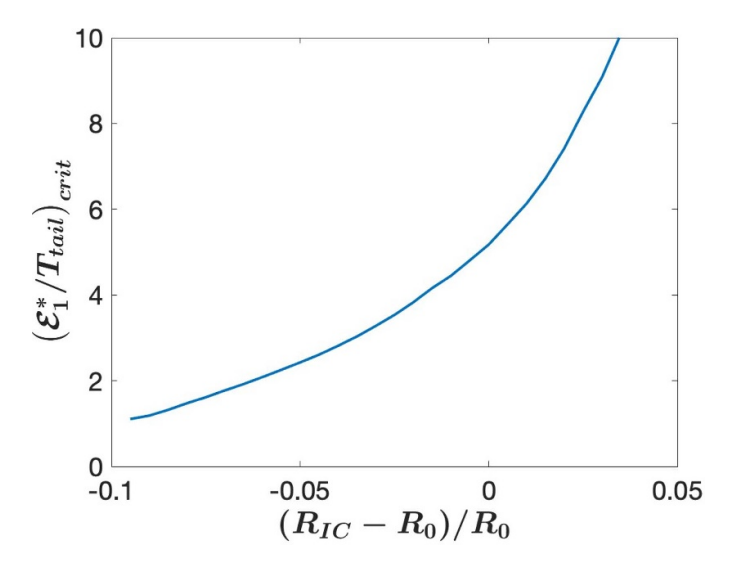


Figure 4. Critical ratio of $\mathcal{E}_1^*/T_{\text{tail}}$ above which $\lambda_{h,1}'$ is positive as a function of the cold ICRF resonance location.

damping. When using our model distribution equation (23) in equation (9), the $\partial f_0/\partial \Lambda$ contribution to $\lambda_{h,1}$, which we denote $\lambda_{h,1,\Lambda}$, takes the form,

$$\lambda_{h,1,\Lambda} = -\zeta \sum_{\sigma} \int \left[\left| \overline{\Upsilon}_{1} \right|^{2} \mathcal{E}^{5/2} \Lambda F(\mathcal{E}, \rho) \frac{\partial g(\Lambda, \rho)}{\partial \Lambda} \right]_{\mathcal{E} = \mathcal{E}_{p}^{*}} \rho d\rho d\Lambda.$$
(25)

In the limit where the width $\Delta\Lambda_{\rm tail}$ tends to zero, such that the distribution function can be approximated by a delta function $\delta(\Lambda-\Lambda_{\rm IC})$, a positive drive of $n_\phi=0$ modes requires that the term multiplying $\partial g(\Lambda,\rho)/\partial\Lambda$ in equation (25) has a positive derivative around $\Lambda=\Lambda_{\rm IC}$. In this limit, one finds after some straightforward algebra,

$$\lambda_{h,p}' = \zeta r \left[\left(\frac{\mathcal{E}_p^*}{T_{\text{tail}}} + \frac{1}{2} \right) \alpha_1 + \alpha_2 \right] |\overline{\Upsilon}_p|^2 \left(\mathcal{E}_p^* \right)^{5/2} F \left(\mathcal{E}_p^* \right)$$
(26)

with,

$$\alpha_1 = \left[\frac{2\Lambda}{h_{\omega_b}} \frac{\partial h_{\omega_b}}{\partial \Lambda} - 1 \right]_{\Lambda = \Lambda_{1C}} \tag{27}$$

and,

$$\alpha_2 = \left[\frac{5\Lambda}{h_{\omega_b}} \frac{\partial h_{\omega_b}}{\partial \Lambda} - \frac{\Lambda}{|\overline{\Upsilon}_p|^2} \frac{\partial |\overline{\Upsilon}_p|^2}{\partial \Lambda} \right]_{\Lambda = \Lambda_{IC}} - 1 \qquad (28)$$

where the coefficients α_1 and α_2 can be easily calculated numerically. These coefficients are functions of ρ and of Λ_{IC} . In the thin banana width limit (with ρ replacing P_{ϕ}), the resonance condition, $\omega_0 = p\omega_b(\mathcal{E}, \Lambda, \rho)$, implies a resonant energy $\mathcal{E}_p^* = \mathcal{E}_p^*(\Lambda_{IC}, \rho; \omega_0)$. One can see from equation (26)

that for instability frequencies corresponding to resonant energies above a critical energy, $\mathcal{E}_{p,\mathrm{crit}}^*$, given by,

$$\mathcal{E}_p^* > \mathcal{E}_{p,\text{crit}}^* = \left(\frac{\alpha_2}{\alpha_1} - \frac{1}{2}\right) T_{\text{tail}}$$
 (29)

there will be a finite contribution from a flux surface to the drive of the $n_{\phi}=0$ mode. In view of the $\mathcal{E}_p^*\propto \omega_0^2$ dependence, equation (29) equates to a condition on the minimum resonant frequency that the energetic ions can drive in the limit of $\Delta T_{\rm tail} \to 0$. A plot of $\mathcal{E}_{1,{\rm crit}}^*/T_{\rm tail}$ as function of resonance position $R_{\rm IC}$ in the midplane for $a\rho/R_0=0.1$ is shown in figure 4. Noting that $\Lambda_{\rm IC}\approx (R_{\rm IC}-R_0)/R_0$, one can see that reasonable values of the critical resonant energy can be obtained for values of $\Lambda_{\rm IC}$ below unity, i.e. when the ICRF resonance is on the high field side. When the resonance is on the low field side, the required values for the instability drive become very high, 5 to 30 times the energy of the tail, which makes effective VDOM destabilisation under such conditions very questionable.

In figure 5, the resonant energy is plotted again as function of ρ for two values of $\Lambda_{\rm IC}$, i.e. $\Lambda_{\rm IC}=1$, corresponding to on-axis ICRF heating, and $\Lambda_{\rm IC}=0.95$, corresponding to ICRF heating on the high field side. Again, one can see that much lower values \mathcal{E}_p^* can drive the $n_\phi=0$ mode for a high field side resonance ($R_{\rm IC}<0$) than for an on-axis resonance ($R_{\rm IC}=R_0$). In fact, the fast ion energy that is required for instability drive in the on-axis resonance case is very high, and for realistic cases the thin banana limit would break down. A weaker instability drive would likely result when nonstandard fast ion orbits are considered. The main conclusion of this analysis is that instability drive is favoured when the ICRF resonance is on the high field side, as the energies of the resonating ions driving the mode are more realistic under such conditions.

It should also be noted that according to equation (29), the critical energy, $\mathcal{E}_{p,\mathrm{crit}}^*$, is independent of the resonant species. In view of the resonant energy having a mass dependence $\mathcal{E}_p^* \propto$

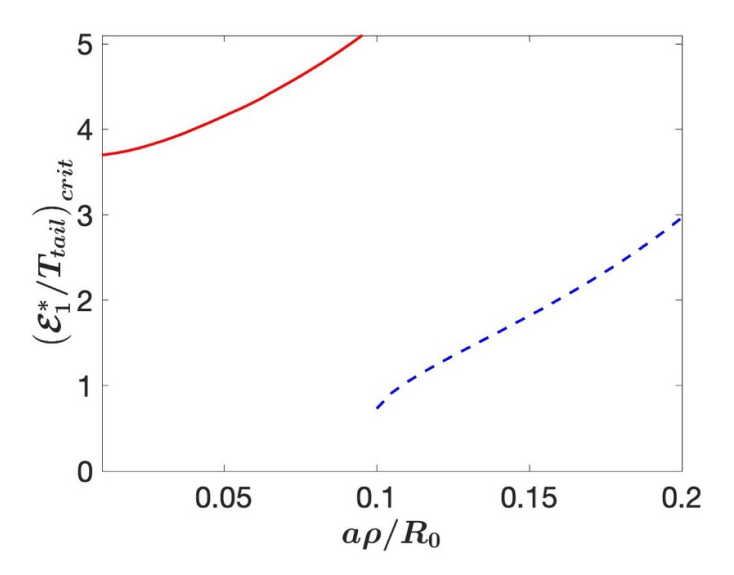


Figure 5. Critical ratio of \mathcal{E}_1^*/T_{tail} above which $\lambda'_{h,1}$ is positive as a function of flux surface radius for $\Lambda_{IC}=1$, red full line, and $\Lambda_{IC}=0.9$ blue dashed line.

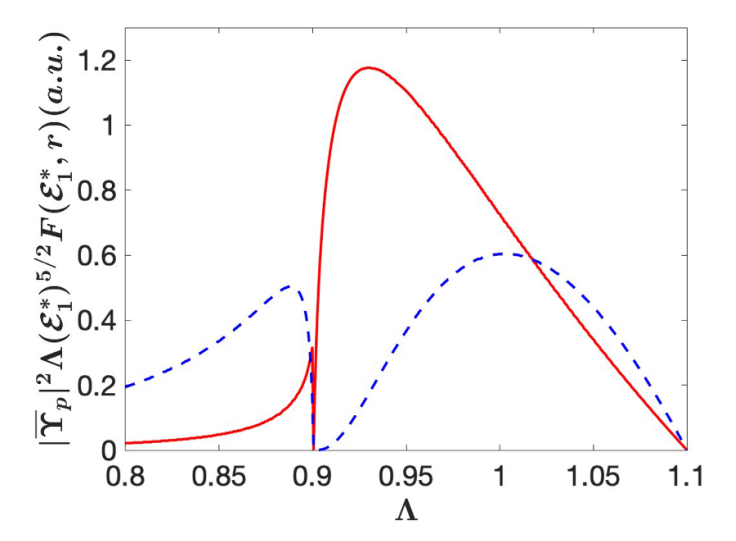


Figure 6. The term multiplying $\partial g(\Lambda,\rho)/\partial\Lambda$ in equation (9). The red solid line corresponds to $\omega_0=100$ kHz and the blue dashed line is for $\omega_0=200$ kHz, the tail energy is $T_{\text{tail}}=600$ keV, and the flux surface where the quantity in the figure is evaluated corresponds to a value $\Lambda_b=0.9$ at the trapped-passing region.

 ω_0^2/m_h , for a given frequency ω_0 which is determined by core plasma parameters, it is clear that for heavier fast ions (e.g. He³ instead of H) the instability drive favours lower values of the mode frequencies ω_0 .

We now turn to the effect of the width of the pitch angle distribution, $\Delta\Lambda_{\rm tail}$, which turns out to be important. In this case a more careful evaluation of the integral in equation (25) is necessary, especially if $\Lambda_{\rm IC}$ falls near the region in phase space corresponding to the trapped-passing boundary at $\Lambda=\Lambda_b$, since the term multiplying $\partial g(\Lambda,\rho)/\partial\Lambda$ in equation (25) varies rapidly in that region. This term is plotted in figure 6 as a function of Λ for two different values of ω_0 , assuming a tail temperature $T_{\rm tail}=600$ keV. The resonating species for both curves is hydrogen. The region of rapid variation of the two curves is at the passing-trapped boundary at $\Lambda_b\approx 0.9$, which corresponds to the flux surface at $a\rho/R_0=0.1$ chosen for this plot (a is the minor radius on the outboard side of the tokamak).

Note that the two curves go to zero for values of Λ corresponding to deeply trapped orbits, i.e. $\Lambda=1.1$ for the parameters of figure 5. This is due to the fact that VDOM are vertical displacements, with $\vec{\xi} \cdot \vec{\kappa} \propto \sin \theta$, and deeply trapped particles are localised at $\theta=0$ (it is an important differentiation factor when comparing the drive of VDOM in this article to $n_\phi=0$ GAE and GAM). At lower frequency (blue dotted curve), the resonant energy is lower and the region of rapid variation around Λ_b (where the curve drops and increases quickly) is not fully resolved, as it is for the red curve obtained for a higher frequency and resonant energy. The key factor that provides for a range with a positive Λ derivative of the term multiplying $\partial g/\partial \Lambda$, in the trapped region, is $F(\mathcal{E}_1^*, \rho)$.

Now, if Δ_{tail} tended to zero, the function $g(\Lambda, \rho)$ would approach $C_g \delta(\Lambda - \Lambda_{IC})$, and then a destabilising contribution would be obtained if the value of Λ_{IC} corresponded to a value of Λ such that the function plotted in figure 6 has a positive

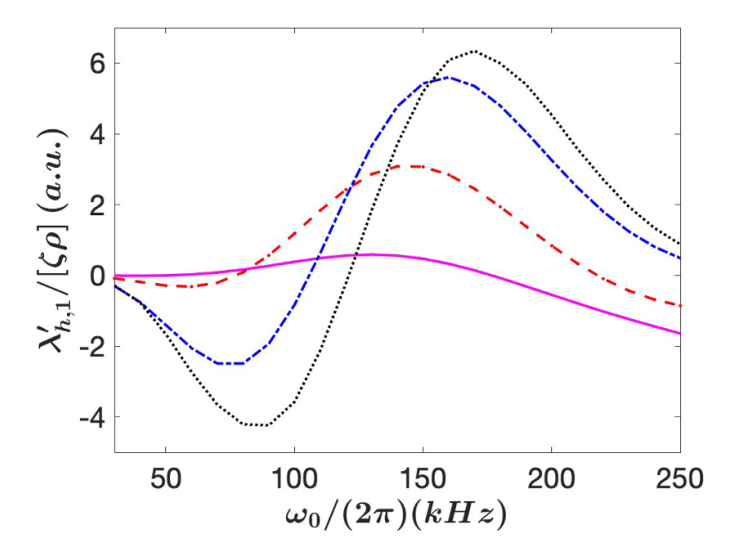


Figure 7. Normalised $\lambda'_{h,1}$ as a function of the resonant frequency for $\Lambda_{IC}=0.94$ and three different values of $\Delta\Lambda_{tail}$: mauve solid line $\Delta\Lambda_{tail}=0.1$, red dashed line $\Delta\Lambda_{tail}=0.05$, blue dot-dashed line $\Delta\Lambda_{tail}=0.025$, and black dotted line a delta function of Λ .

slope, as pointed out before (but note that the damping contribution from $\partial F(\mathcal{E},\rho)/\partial \mathcal{E}$ term must be overcome for the aggregate to result in destabilisation). However, if the interval of Λ values of width $\Delta\Lambda_{tail}$ around Λ_{IC} included regions of positive and negative slopes, then a more careful balance represented by the integral in equation (25) may lead to a reversal of the result obtained in the limit of $\Delta\Lambda_{tail} \to 0$, which is shown below.

In order to study this point, we have used the distribution given by equation (23) together with a full numerical integration according to equation (9). The result is shown in figure 7 for a case of ICRF-accelerated hydrogen minority ions with $\rho a/R = 0.1$, R = 3m, q = 1.05 (safety factor at the considered flux surface), $T_{\text{tail}} = 600 \,\text{keV}$, $\Lambda_{\text{IC}} = 0.94$ (which corresponds to a flux surface that crosses the inner mid-plane just to the high field side of R_{IC}) and four different widths: $\Delta \Lambda_{\text{tail}} = 0.1$, $\Delta \Lambda_{\text{tail}} = 0.05$, $\Delta \Lambda_{\text{tail}} = 0.025$ and a delta function $g(\Lambda)$.

One can see from figure 6 that the term multiplying $\partial g/\partial \Lambda$ has a negative slope at $\Lambda = 0.94$ for the $\omega_0/(2\pi) = 100\,\mathrm{kHz}$ case. Consequently, damping is expected when $\Lambda_{IC} = 0.94$ in the case of a very narrow pitch angle distribution $g(\Lambda, \rho)$. This is indeed the case, as can be seen in figure 7. However, when the width of the pitch angle distribution is increased, destabilisation of VDOM occurs at some point. Figure 7 shows that a finite drive of the VDOM at $\omega_0/(2\pi) = 100$ kHz is present for $\Delta\Lambda_{\text{tail}} = 0.05$. A key factor behind the drive of the mode with this wider pitch angle distribution is that a fraction of the resonating ions are in the passing region. It is clear from figure 6 that for $\omega_0/(2\pi) = 100$ kHz the passing ions only contribute weakly in the direction of damping the VDOM, while the contribution from the drive for $\Lambda > \Lambda_{IC}$ is comparatively strong. On the other hand, the figure also shows that when the width is further increased, the strength of the drive is diminished. This is because the spread is too large and the contribution from energetic ions with $\Lambda \gtrsim 1$ to the drive is comparatively weak.

An important point is the characteristic energies of the energetic ions that effectively contribute to the drive of the VDOM. An indication can be obtained by plotting $\lambda'_{h,1}$ as a function of the resonant energy evaluated at $\Lambda=\Lambda_{IC},$ i.e. $\mathcal{E}_1^*(\omega_0,\Lambda_{IC},\rho)$. The result for the case of $\Delta\Lambda_{tail}=0.05$ is shown in figure 8.

In the frequency range up to around $\Omega_0 = 150\,\mathrm{kHz}$ (i.e. roughly up to where $\lambda'_{h,1}$ is maximum), figure 8 shows that fast-ion VDOM instability drive peaks for energies just below $2\,\mathrm{MeV}$.

After this basic analysis of the potential for ICRF accelerated ion to drive $n_{\phi} = 0$ VDOM modes, we now examine a full simulation of the energetic ion distribution with the PION code in accordance with the model presented in appendix B. The main parameters used for the PION simulation are as follows: H minority heating in a JET sized deuterium plasma, (H)D, with a magnetic field on axis of $B_0 = 3$ T; a density profile $n_{\rm e}(\rho) = (n_{\rm e,0} - n_{\rm e,edge})(1 - \rho^2)^{0.5} + n_{\rm e,edge}$, with $n_{\rm e,0} = 3.5 \cdot 10^{19}$ and $n_{\rm e,edge} = 4 \cdot 10^{18}$; $T_{\rm e}(\rho) = T_{\rm i}(\rho) =$ $(T_{e,0} - T_{e,edge})(1 - \rho^2) + T_{e,edge}$, with $T_{e,0} = 6 \text{ keV}$ and $T_{\rm e,edge} = 0.5 \, \rm keV$; the ICRF frequency is $f = 50 \, \rm MHz$ (placing the fundamental hydrogen resonance, $\omega_{\rm IC} \approx \omega_{c,H}$, on the high field side and intersecting the mid-plane around $\rho = 0.3$); an ICRF power of $P_{RF} = 8 \text{ MW}$; the antenna spectrum used is representative of dipole phasing in JET. According to the simulation, about 80% of the ICRF power is absorbed by the hydrogen minority ions, 9% by the deuterium ions (second harmonic absorption) and 11% by the electrons (through electron Landau damping and transit time magnetic pumping). The deposition profile of the hydrogen ions is shown in figure 9.

The figure shows that the power density peaks a little inside $\rho = 0.3$ (an effect of the Doppler broadening of the ICRF resonance). The contribution to $\lambda'_{h,1}$ from flux surface $\rho = 0.25$ is shown in figures 10 and 11. According to the PION calculations, the averaged 'tail temperature' of the resonating hydrogen ions was about 400 keV on this flux surface. It therefore comes as no surprise that the contribution resembles those obtained with the model distribution above.

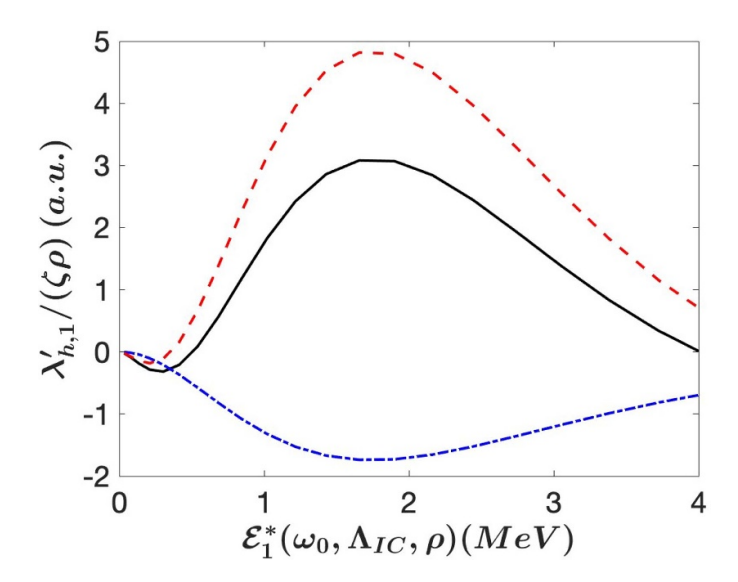


Figure 8. Normalised $\lambda'_{h,1}$ black line as a function \mathcal{E}_1^* evaluated at $\Lambda = \Lambda_{\rm IC}$; the blue line is contribution from the $\partial f_0/\partial \mathcal{E}$ term, the red line is the contribution from the $\partial f_0/\partial \Lambda$ term.

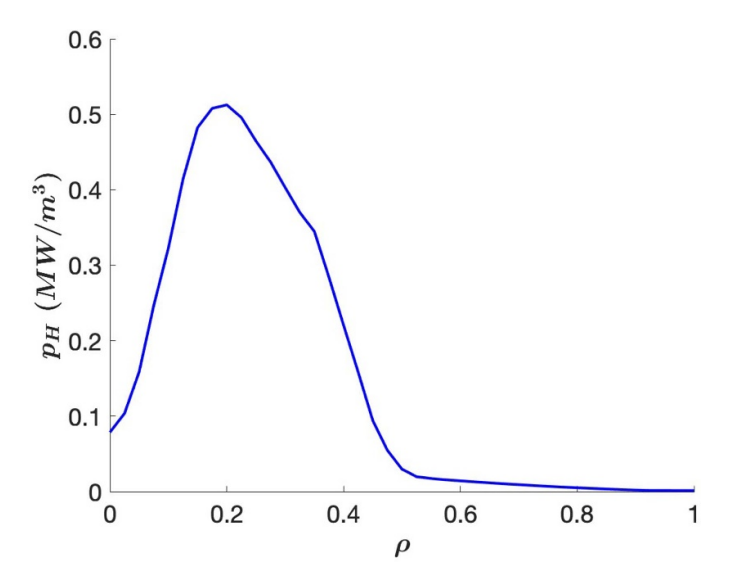


Figure 9. Power density, p_H , absorbed by the hydrogen minority ions as a function of the flux surface label ρ .

The peak of $\lambda'_{h,1}$ is found around 125 kHz, which translated into the resonant energy, \mathcal{E}_1^* evaluated at $\Lambda = \Lambda_{IC}$ of around 2 MeV. One can also see that there is effective damping from above 200 kHz, corresponding to particles roughly above 4 MeV.

The typical tail temperature of the energetic ions in current simulations (\sim 400 keV) is relatively moderate, and the width of the orbits of the resonating energetic ions should therefore be comparatively modest. Consequently, the adopted thin banana width approximation should provide results that are, at least qualitatively, reasonable for an initial exploration of the drive of n_{ϕ} modes through the anisotropy of ICRF accelerated energetic ions.

To have the complete picture it is of course essential to calculate $\lambda_{h,1}$ itself, i.e. evaluating the integral of d $\lambda'_{h,1}$ over all flux surfaces and the constant ζ for the parameters used in the PION simulation. The resulting $\lambda_{h,1}$ is shown in figure 12 as

a function of the frequency ω_0 . As can be seen, the potential drive is up to frequencies around $\omega_0/(2\pi)=175$ kHz. At $\omega_0/(2\pi)=150$ kHz we have $\lambda_{h,1}\approx 0.7$, which corresponds to a contribution to the growth rate of $\omega_0\lambda_{h,1}/2\approx 3.8\cdot 10^5$ 1/s. This value exceeds the estimated value of the damping for typical JET parameters reported in [14].

The conclusion of this section is clear: a significant drive of the $n_{\phi}=0$ VDOM only occurs for ICRF resonance on the high-field side. A key effect is the dispersion of particles into the passing region, which is caused by collisional pitch angle scattering. The passing fraction of the energetic ions only weakly contributes to reducing the drive of the mode up to moderate instability frequencies, resulting in a dominant drive of the VDOM by energetic ions with $\Lambda \gtrsim \Lambda_{\rm IC}$. For parameters representative of a JET like device, $\lambda_{h,1}$ is found to be sufficiently high at frequencies up to around 150 kHz to drive a VDOM.

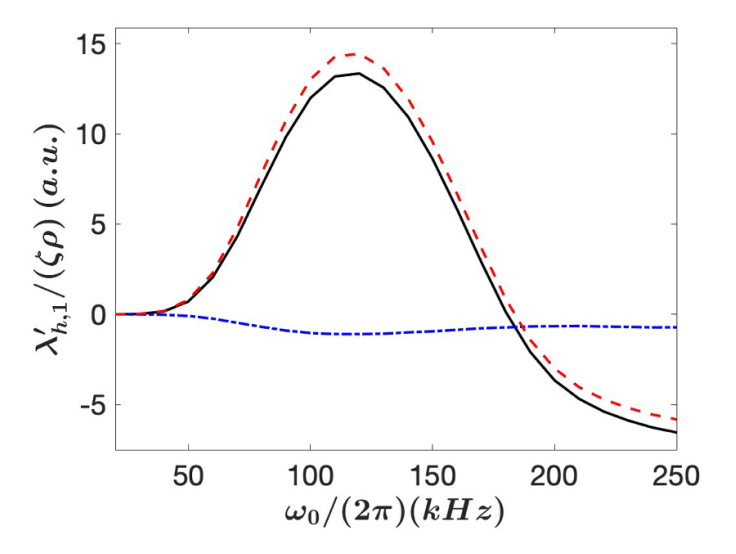


Figure 10. Normalised $\lambda'_{h,1}$ at $\rho = 0.25$ as a function of the instability frequency, black solid line; the blue line is contribution from the $\partial f_0/\partial \mathcal{E}$ term, the red line is the contribution from the $\partial f_0/\partial \Lambda$ term.

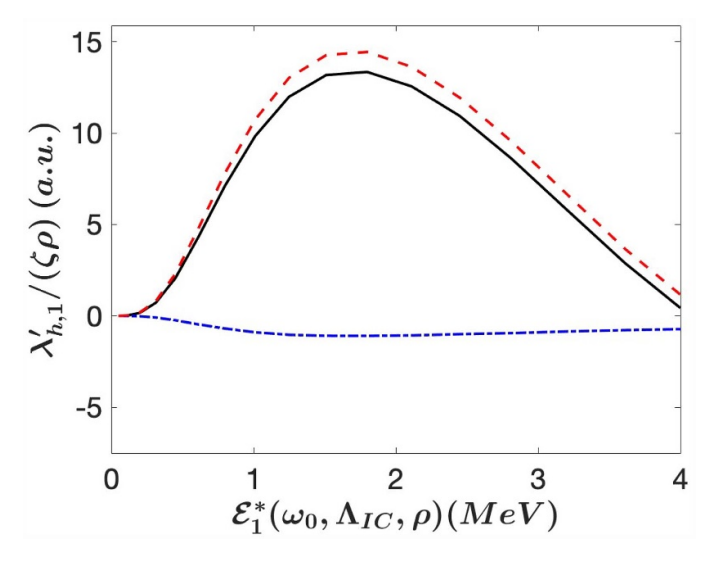


Figure 11. Normalised $\lambda'_{h,1}$ at $\rho = 0.25$ as a function of the resonant energy evaluated at $\Lambda = \Lambda_{\rm IC}$, black solid line; the blue line is contribution from the $\partial f_0/\partial \mathcal{E}$ term, the red line is the contribution from the $\partial f_0/\partial \Lambda$ term.

In the next section, we will investigate if a transient inversion of the distribution function in the energy direction following a sawtooth crash can drive modes more effectively for on-axis resonances.

6. Sawtooth redistribution of energetic ions

During a sawtooth crash and subsequent reconnection, the hot core plasma inside the q=1 surface is mixed with the colder plasma outside within the so-called mixing radius. This plasma redistribution is a result of the reconnecting magnetic field and the fact that most low to moderate energy plasma particles are tied to the field lines. However, energetic trapped ions have wider orbits and process in the toroidal direction, i.e. they experience different phases of the MHD perturbation associated with the sawtooth instability. Consequently, energetic ions, especially trapped ones, can be expected to be less

redistributed than thermal ones [19]. A criterion for the energy of ions where they start to experience reduced redistribution was given in [19] as,

$$\mathcal{E}_{\text{crit}} = 2\pi m_h k_s r_s R_0 \omega_b / \tau_{\text{cr}}$$
 (30)

where m_h is the mass of the energetic ion species; k_s is the ellipticity and r_s is the radius at the q=1 surface; ω_b is the bounce frequency; and $\tau_{\rm cr}$ is the sawtooth crash time. Of course $\mathcal{E}_{\rm crit}$ does not represent a sharp boundary, and for detailed studies it is necessary to follow energetic particles in the perturbed fields associated with the sawtooth crash [19, 20]. The study in [20] indicates that the transition region in energy, $\Delta \mathcal{E}_{\rm tran}$, may extend up to the order of $0.5\mathcal{E}_{\rm crit}$. There is naturally also a difference between trapped and passing fast ions, but because most energetic ions accelerated by ICRF heating tend to be trapped, for this work we only need to consider the critical energy for the trapped ions given in equation (30).

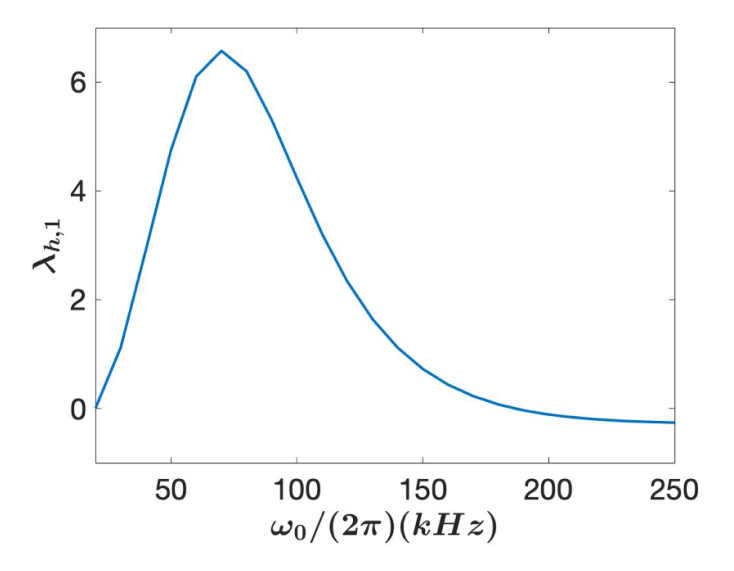


Figure 12. $\lambda'_{h,1}$ as function of the instability frequency.

In order to take into account that the trapped ions above the critical energy $\mathcal{E}_{\text{crit}}$ are becoming less and less redistributed, it is assumed that only a fraction of the fast ions are redistributed at each energy level $F_{\text{Redist}}(\mathcal{E})$, and an ad hoc expression is used.

$$F_{\text{Redist}}(\mathcal{E}, t_{-}) = F(\mathcal{E}, t_{-}) \left\{ 1 - \left[\frac{1}{2} + \frac{1}{\pi} \arctan\left(\frac{\mathcal{E} - \mathcal{E}_{\text{crit}}}{\Delta \mathcal{E}_{\text{tran}}} \right) \right] f_{\text{trapped}} \right\}$$
(31)

where $Mv_{\rm crit}^2/2 = \mathcal{E}_{\rm crit}$ and t_- indicate a time point just before the sawtooth crash. Thus, when a sawtooth crash is applied in the code, the $F_{\rm Redist}(\mathcal{E},t_-)$ is sent to the redistribution model, which calculates the post sawtooth redistributed distribution function, $F_{\rm Redist}(\mathcal{E},t_+)$. The normal PION simulations are then resumed with,

$$F(\mathcal{E}, t_{+}) = F(\mathcal{E}, t_{-}) \left[\frac{1}{2} + \frac{1}{\pi} \arctan\left(\frac{\mathcal{E} - \mathcal{E}_{\text{crit}}}{\Delta \mathcal{E}_{\text{tran}}}\right) \right] f_{\text{trapped}} + F_{\text{Redist}}(\mathcal{E}, t_{+}).$$
(32)

We use the model outlined in [30] to redistribute the energetic ions prescribed by equation (31). It assumes a Kadomtsev reconnection and that the redistributed ions follow the reconnecting field lines.

In the current paper, we neglect finite orbit width effects in the Fokker–Planck calculations. This is of course a limitation because ICRF accelerated ions in a machine like JET tend to acquire energies in the MeV range during high power heating. On the other hand, the critical energy \mathcal{E}_{crit} is typically of the order of 500 keV for representative ICRF heated JET plasma [19] and at such energies finite orbit width effects should be moderate. Thus, for this initial assessment of inverted energy distributions, neglecting finite orbit width effects should be acceptable. It should also be noted that our model for the anisotropy of the distribution function is adapted to the phase before a crash, while some differences are expected in

the post crash phase that are not captured by our simplified modelling. Thus, there is room for improvement by using more complex modelling. However, we do not expect it to affect the general conclusions of the simulations presented below.

7. Analysis of locally energy inverted distributions following sawtooth redistribution

In order to assess the impact of sawtooth crashes on the energy distribution of ICRF accelerated ions, full PION simulations have been carried out, using the model in appendix B and the sawtooth redistribution model described in the previous section. As a base case, minority on-axis heating of 3 He ions in a deuterium plasma, (3 He)D, is considered, with an ICRF frequency of f = 30.5 MHz and other plasma parameters the same plasma as used in section 5. Here, it should be noted that on-axis heating is the most relevant because sawtooth redistribution for off-axis resonances would not have the same impact on the energy distribution of the energetic ions.

We first consider a case with the q=1 surface before the sawtooth crash located at $\rho=0.22$, a minority ion concentration $n_{^3\mathrm{He}}/n_\mathrm{D}=4\%$, $P_\mathrm{RF}=6\,\mathrm{MW}$, a critical energy $\mathcal{E}_\mathrm{crit}=500\,\mathrm{keV}$, and $\Delta\mathcal{E}_\mathrm{tran}=0.1\mathcal{E}_\mathrm{crit}$. The simulations are driven up to a near steady state before the sawtooth crash is applied. The profile of the power density absorbed by the resonating $^3\mathrm{He}$ ions just before the crash is shown in figure 13. This figure shows that in the simulation most of the ICRF power is absorbed within the assumed q=1 surface.

Figure 14 shows the pitch angle averaged distribution function at $\rho = 0.1$ just before and after the sawtooth crash. As can be seen, the post crash distribution function has a positive energy slope below the critical energy. The reason is that because of the peaked ICRF power deposition profile, the distribution near the centre has more energetic particles in the region around 100 to 500 KeV than distribution functions on flux surfaces outside the q=1 surface. Consequently, when the region below $\mathcal{E}_{\text{crit}}$ becomes redistributed in the sawtooth

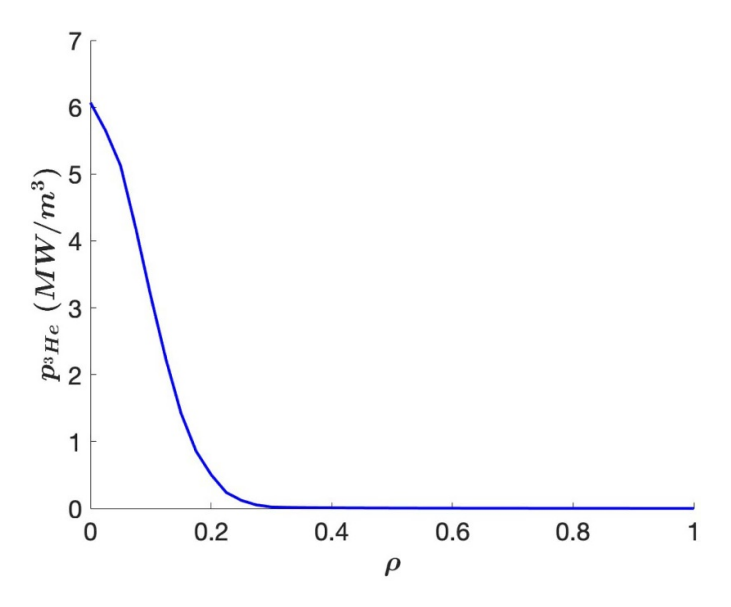


Figure 13. ICRF power deposition profile of the resonating ³He ions just before a sawtooth crash is applied.

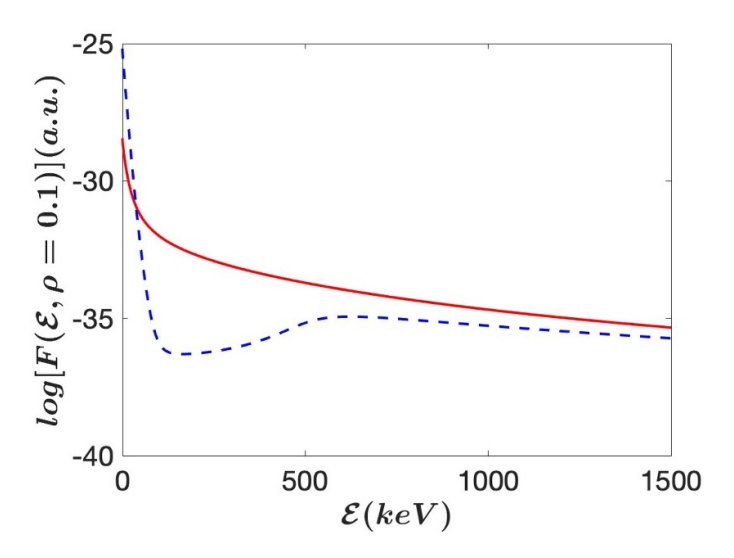


Figure 14. Pitch angle averaged distribution function just before the sawtooth crash, solid red line; and just after the crash dashed blue line.

crash, the energetic particles below \mathcal{E}_{crit} are expelled and there is an influx of colder particles originating from outside of q = 1.

Following the sawtooth crash, the ICRF induced velocity space diffusion drives the distribution function back towards being monotonic. The positive slope of the energy distribution will only exist rather transiently. This is shown in figure 15, which shows $max[\partial F(\mathcal{E}, \rho=0.1)/\partial \mathcal{E}, 0]$, where the 'max' function signifies values greater than zero. A positive slope of the distribution function is only maintained for about 25 ms. Of course, this is assuming that the sawtooth period is longer than the time period during which the distribution is locally energy inverted.

One can conjecture that the main factor influencing the period during which the a locally energy inverted distribution can be maintained is the ICRF induced velocity space diffusion. Roughly speaking, the time scale on which the inversion can be maintained is of the order of the time it takes for a resonant ion to traverse the inverted region due to velocity space diffusion. Because we are dealing with a diffusive process, a particle will explore a velocity region of the order of $\Delta v \pm \sqrt{2D_{\text{RF}}\Delta t}$ during a period Δt , where D_{RF} is the ICRF diffusion coefficient in velocity space. If we neglect finite Larmor radius (FLR) effects, it is given by [29],

$$D_{\rm RF} \approx \frac{p_{RF}}{3n_{\rm res}m_{\rm res}},\tag{33}$$

where n_{Res} is the density of the resonating minority ions, m_{res} is their mass, and p_{RF} is the absorbed flux-surface-averaged power density. The excursion in velocity gives rise to an excursion in energy,

$$(\Delta \mathcal{E})^2 \sim \mathcal{E} \frac{4p_{\rm RF}}{3n_{\rm res}} \Delta t.$$
 (34)

Thus, the time it will take to explore a region of energy space of the order of the critical energy after which the distribution

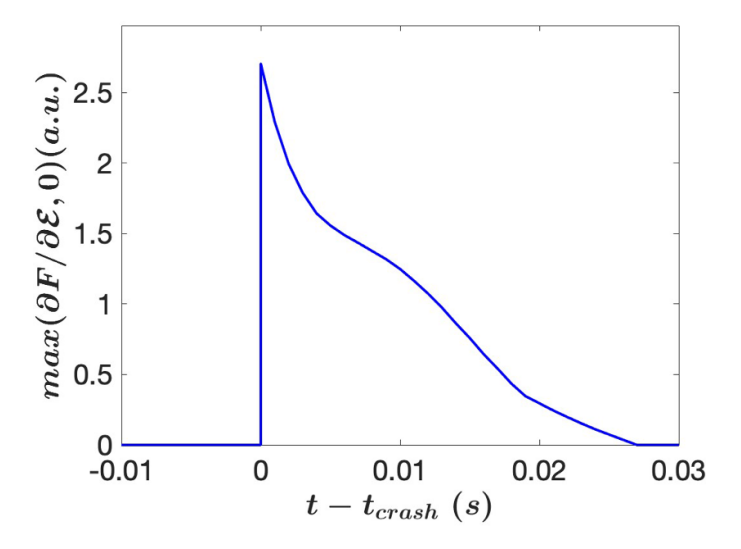


Figure 15. max value of $\partial F/\partial \mathcal{E}$ taken over all flux surfaces and energy levels.

should have been returned to monotonic is roughly given by,

$$\Delta t_{\rm inv} \sim \mathcal{E}_{\rm crit} \frac{3n_{\rm res}}{4p_{\rm RF}}.$$
 (35)

In the simulation with $P_{\rm RF}=6\,{\rm MW}$, the typical power density absorbed by the hydrogen minority ions in the centre of the plasma is around $p_{\rm RF}=3\,{\rm MW\,m^{-3}}$ (i.e. near $\rho=0.1$, see figure 13), and for a minority concentration of 4% we have $n_{^3{\rm He}}=1.1\cdot10^{18}\,{\rm m^{-3}}$. If we insert these parameters in the formula above with $\mathcal{E}_{\rm crit}=500\,{\rm keV}$ we obtain $\Delta t_{\rm inv}\approx12\,{\rm ms}$, which is the right order of magnitude. Thus, this elementary analysis indicates that the duration of a region with $\partial F(s,\mathcal{E},t)/\partial\mathcal{E}>0$ is largely set by the ICRF induced velocity space diffusion, with the minority density and the absorbed power density playing key roles.

In order to further explore the duration and the radial extent of a region with $\partial F(\rho, \mathcal{E}, t)/\partial \mathcal{E} > 0$ following a sawtooth crash, we have carried out simulations with scans in ICRF power and the minority density. Two types of power scans have been performed, one in which all parameters except the power have been kept constant and the second in which the ratio $P_{\rm RF}/n_{\rm res}$ has been kept constant. The results of the power scans can be seen in figure 16.

The power scans show that the duration of the inverted energy distribution decreases with ICRF power if the minority concentration is kept constant. In fact, it decreases more quickly with power than the simple estimate equation (35) suggest. One should note that above a power of about $P_{\rm RF}=12\,{\rm MW}$ it is no longer possible to create a positive slope of the distribution function in the centre of the plasma. The reason for this is that at high power levels, a sufficiently strong tail on the distribution function develops also outside the q=1 radius, such that enough energetic ions are redistributed towards the centre to prevent a region with $\partial F(\rho,\mathcal{E},t)/\partial \mathcal{E}>0$. The scan with $P_{RF}/n_{\rm minority}$ held constant shows much less variation with the RF power as expected from the simple estimate of equation (35). These scans support the notion that $P_{\rm RF}/n_{\rm minority}$ is indeed a key factor determining the duration under which a

region with an inverted energy distribution persists following a sawtooth crash. However, it is of course the case that the physics is more complicated than suggested by the simple estimate given in equation (35). For instance, the change of minority concentration leads to a modification of the polarisation of the ICRF waves, which in its turn affects the details of the ICRF diffusion coefficient (it plays a role already at energies of a few hundred keVs). Furthermore, effects such as the nonlinear change of the power deposition owing to high energy tails on the resonating ion distribution functions also have an effect. Obviously, these types of effects are difficult to capture in a simple expression.

The width of the transition region around \mathcal{E}_{crit} between strong and weak redistribution determines the extent of the region of velocity space for which the fast particle distribution can have a positive slope as a function of energy. This is illustrated in figure 17, which shows the maximum of $(\partial F/\partial \mathcal{E})$ just after the sawtooth crash as a function of the radial coordinate for widths $\Delta \mathcal{E}_{tran}$ corresponding to a transition region in energy, $\Delta \mathcal{E}_{tran}$, of $0.1\mathcal{E}_{crit}$, $0.2\mathcal{E}_{crit}$, $0.3\mathcal{E}_{crit}$, and $0.4\mathcal{E}_{crit}$. As expected, the radial extent of the region with an energy-inverted distribution is within the mixing radius $(\rho_{\rm mix}=0.3)$, and both the radial region and the magnitude of $\partial F/\partial \mathcal{E}$ decrease as the transition region gets wider in energy. For values of $\Delta \mathcal{E}_{tran} \ge 0.5 \mathcal{E}_{crit}$, energy-inverted distributions no longer appear. Thus, in view of the results presented in [20], it may indeed be the case that for realistic values of the width of the transition region it will not be easy to produce bumpon-tail-like distributions of fast ions with $\partial F(\rho, \mathcal{E}, t)/\partial \mathcal{E} > 0$.

It is also of interest to investigate how the critical energy influences the locally inverted energy distribution. Not least because the sawtooth crash time can vary significantly and the critical energy is inversely proportional to it. Figure 18 shows the distribution function before and after redistribution for a case with $\mathcal{E}_{\text{crit}}=1.5$ MeV. As can be seen, the distribution again becomes hollow, but the region with positive slope is fairly shallow, and the maximum of $\partial F/\partial \mathcal{E}$ is therefore relatively weak.

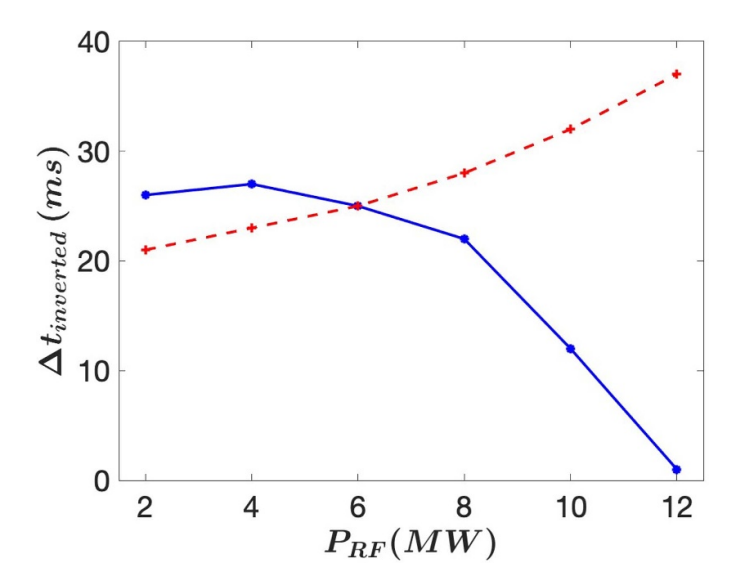


Figure 16. Duration of inverted energy distribution as a functions of ICRF power, blue points (and curve) are with a constant minority density of 4% whereas the red crosses (and curve) are for when P_{RF}/n_{min} has been held constant.

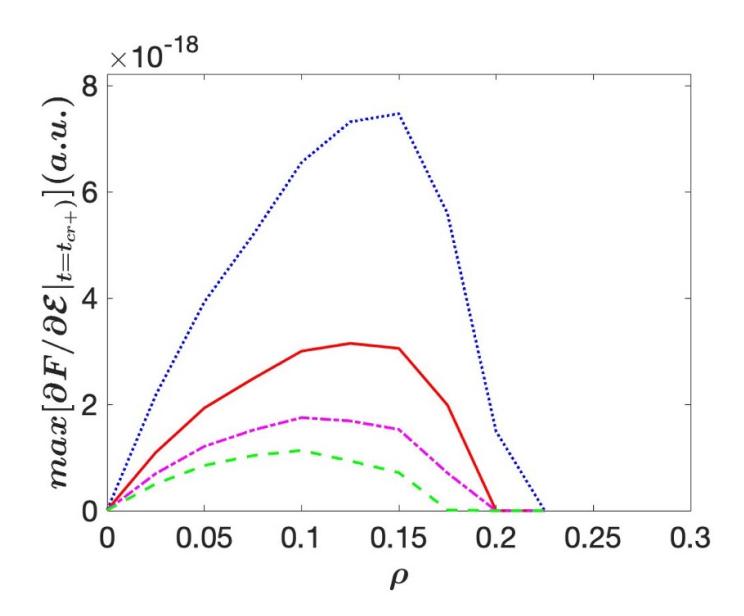


Figure 17. Max value of $\partial F/\partial \mathcal{E}$ over all energy levels just after the sawtooth redistribution has taken place for $\Delta \mathcal{E}_{tran} = 0.1 \mathcal{E}_{crit}$, dotted line, $\Delta \mathcal{E}_{tran} = 0.2 \mathcal{E}_{crit}$ solid line, $\Delta \mathcal{E}_{tran} = 0.3 \mathcal{E}_{crit}$ dashed line and $\Delta \mathcal{E}_{tran} = 0.4 \mathcal{E}_{crit}$ dash dotted line.

The radius of the q=1 surface when a sawtooth is triggered in a tokamak can vary significantly. In particular, the presence of energetic ions can lead to so-called monster sawteeth, which are characterised by longer periods between crashes and larger radii of the q=1 surface. We have therefore run simulations with different q=1 radii. It is found that the bump on tail feature is not much affected by the q=1 radius provided that most of the ICRF power deposition falls inside this radius. On the other hand, for q=1 radii smaller than the deposition width, the local inversion of the distribution function in the energy direction becomes less pronounced.

The results presented in this section indicate that a locally inverted, bump-on-tail-like distribution in the energy direction of ICRF accelerated ions can form as a result of sawtooth redistribution. However, the distribution will remain inverted for a fairly short period of time. Furthermore, there is significant uncertainty regarding the width of the transition region in energy between redistributed ions and those that suffer very little redistribution. In the next section, we investigate the potential for VDOM modes to be driven by sawtooth-induced energy-inverted distributions assuming $\Delta \mathcal{E}_{tran} = 0.1 \mathcal{E}_{crit}$ to ensure a significant inversion.

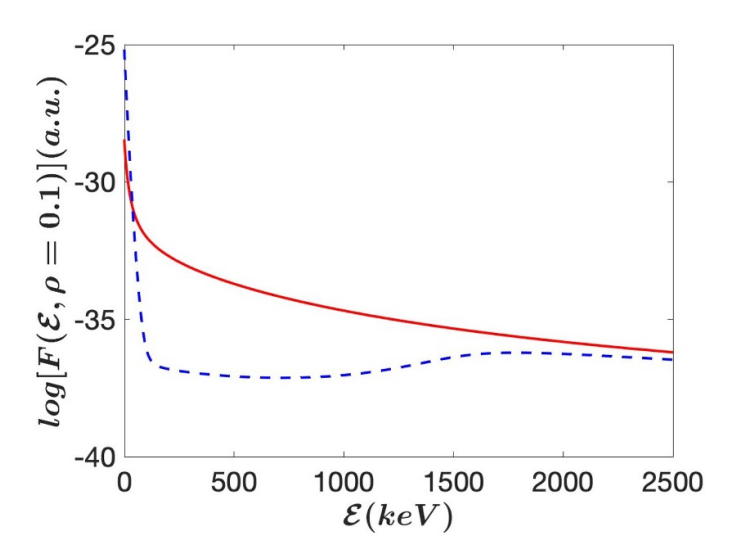


Figure 18. Pitch angle averaged distribution function for $\mathcal{E}_{crit} = 1500 \, \text{keV}$ just before the sawtooth crash, solid red line; and just after the crash dashed blue line.

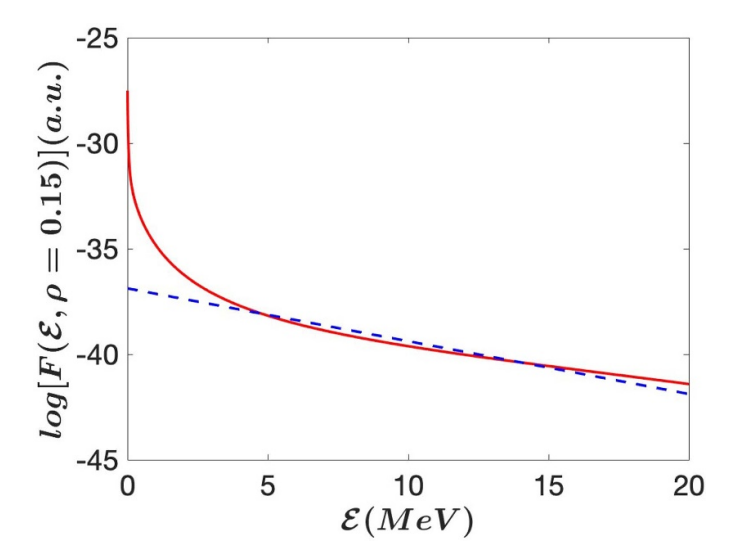


Figure 19. Pitch angle averaged distribution function just before the sawtooth crash, solid red line; and a Maxwell distribution with a 'tail temperature' of 4 MeV.

8. Numerical evaluation of the $n_\phi=0$ drive for locally energy inverted energetic ion distributions following a sawtooth crash

In this section we study the instability drive for the distribution functions simulated by PION in the previous section. First, the simulated distribution function just before the sawtooth crash is considered. We limit ourselves to looking at the contribution from a single flux surface $\rho = 0.15$, corresponding to $r/R_0 \approx 0.04$ for a JET like plasma. The simulated distribution function at this flux surface is shown in figure 19 together with a Maxwellian with a temperature of 4 MeV arranged to roughly coincide with the high energy tail of the simulated distribution function. As can be seen, the 4 MeV Maxwellian fits the high energy tail beyond 5 MeV quite well. It should, however, be noted that the averaged 'temperature' of the whole distribution function defined

 $w_{^3\text{He}} = (3/2) n_{^3\text{He}}kT_{av}$ is calculated to be around 600 keV. It is largely the strong FLR effects in the RF-diffusion coefficients for (^3He)D heating that are responsible for the high asymptotic tail temperature. The analysis of section 5 suggests that in the current case instability drive would become important at resonant energies \mathcal{E}_1^* of the order of 15–20 MeV, i.e. 4–5 times higher than the asymptotic tail temperature at 4 Mev. The resonant energy for particles with turning points at the cold ICRF resonance, i.e. $\Lambda = 1$ for on axis heating, is shown in figure 20. It shows that an instability in this energy range would correspond to an instability frequency of around 200 kHz.

The result of calculating $\lambda_{h,1}$ as a function of the instability frequency with the simulated distribution function and equation (9) is shown in figure 21. In line with the simple estimate above, the figure shows that there is an instability drive for frequencies slightly above 200 kHz. In this context

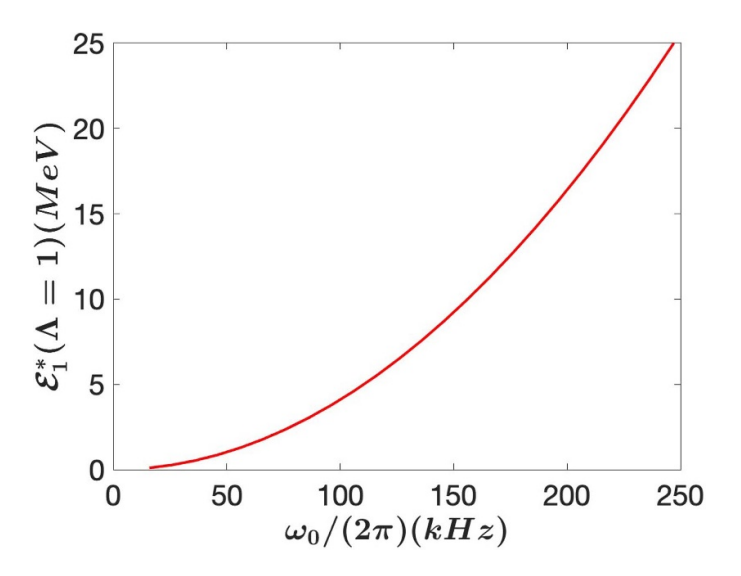


Figure 20. Resonant energy as a function of the instability frequency.

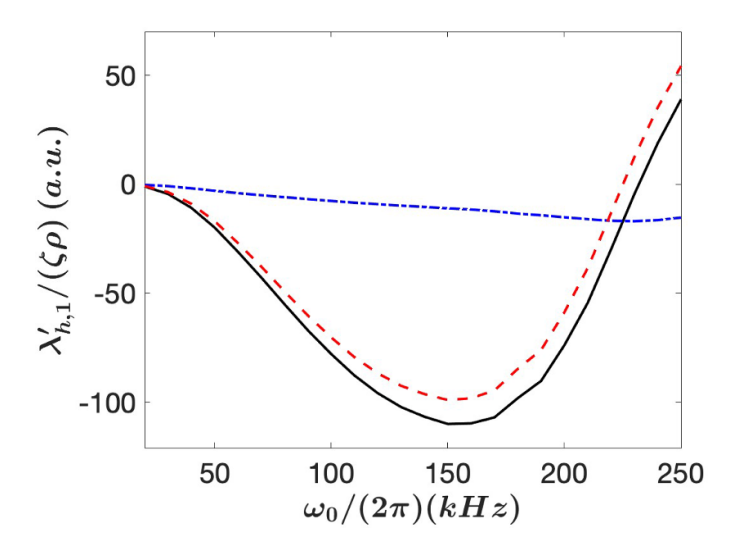


Figure 21. Normalised $\lambda_{h,1}$, red line, as a function of the instability frequency just before the sawtooth redistribution. The blue and black lines are the contributions from the $\partial f_0/\partial \mathcal{E}$ and $\partial f_0/\partial \Lambda$ equation (9) respectively.

it should be remarked that the number of particles in the 15–20 MeV range is small, and it goes without saying that the small banana width approximation adopted here completely breaks down in the energy range where the resonant ions contribute to drive. However, more accurate estimates are beyond the scope of this exploratory study and will have to be left for future work.

The question is now whether the locally inverted distribution function in the energy direction is sufficient to drive the $n_{\phi}=0$ instability considered here. It turns out that using the post crash distribution makes little difference to the overall picture presented in figure 21, the damping because of the $\partial f/\partial \Lambda$ is almost unchanged and dominates. The contribution from the $\partial f/\partial \mathcal{E}$ term remains small and in order to see difference between the pre and post crash contribution more clearly the contribution from $\partial f/\partial \mathcal{E}$, which we denote by $\lambda_{h,1,\mathcal{E}}$, is shown in figure 22.

There is a distinct difference, before the redistribution the $\partial f/\partial \mathcal{E}$ term clearly contributes to the damping of the VDOM while just after the redistribution it provides an almost neutral contribution for frequencies up to around 70 kHz. Here it should be noted that \mathcal{E}_1^* is around 1 MeV for $\Lambda=1$ and $\omega_0 \approx 80\,\mathrm{kHz}$, i.e. one can clearly identify the impact of the energy inverted region on $\lambda_{h,1,\mathcal{E}}$. However, the contribution of the bump on tail feature is not sufficient to drive the instability, especially because the values of $\partial f_0/\partial \Lambda$ have a strong damping effect in the energy region in question. Furthermore, the width of the pitch angle distribution in this energy range is not negligible. As a result, the Λ integral in equation (9) spans a rather wide \mathcal{E}_1^* range and the driving contribution of the energy inverted region is virtually cancelled by contributions of the regions outside it. Several values of \mathcal{E}_{crit} have been analysed and in none of the cases was the inversion in the energy distribution sufficient to overcome the damping provided by the $\partial f_0/\partial \Lambda$ term.

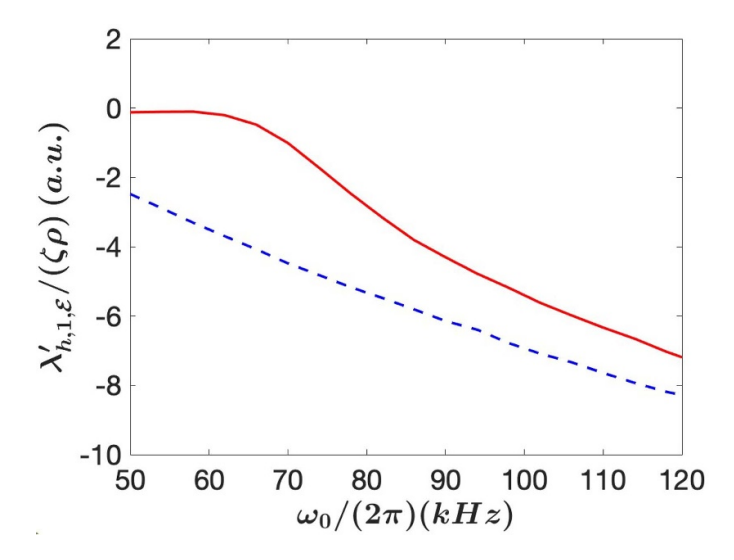


Figure 22. Normalised contribution, $\lambda_{h,1,\mathcal{E}}$, from the $\partial f/\partial \mathcal{E}$ term to $\lambda_{h,1}$ as a function of the instability frequency, the blue dashed line is the contribution from just before the sawtooth redistribution while the red line is from just after the redistribution.

Thus, the conclusion is that while ICRF accelerated ions in a JET-like device could have a locally energy inverted distribution function following a sawtooth crash, this is not sufficient to drive the considered $n_{\phi}=0$ vertical mode, at least for the cases studied here. Of course, it should be emphasised that this finding is specific to ICRF accelerated energetic ions that are mainly trapped with a narrow pitch angle distribution.

9. Conclusions

The potential for ICRF accelerated energetic ions to drive $n_{\phi}=0$ VDOMs in a tokamak has been investigated. In principle, they could drive these modes either because of the anisotropy in velocity space that characterises ICRF-accelerated ions, or through locally inverted distribution functions in the energy direction. The latter could arise transiently because of particle redistribution during a sawtooth relaxation. A condition is that more trapped energetic particles are less redistributed than lower energy ones, which has been suggested to be the case [19].

The PION code has been used to simulate distribution functions of ICRF accelerated ions, and they have subsequently been used as input to linear stability calculations of the drive of $n_{\phi}=0$ VDOM. A key feature of this code is that it allows for time dependent simulations on a routine basis, which is necessary for evaluating distribution functions following a sawtooth crash. Because the anisotropy of the distribution function plays a key role, the standard PION code has been augmented with a routine for approximately reproducing the 'rabbit-ear' shape, see e.g. [28], of the level surfaces of the distribution function. Moreover, a simple model, with a transition region around a critical energy $\mathcal{E}_{\text{crit}}$, has been used to simulate the redistribution of the ICRF accelerated ions following a sawtooth crash assuming a Kadomtsev type reconnection.

The main conclusion of the presented study is that the anisotropy of the distribution function of ICRF heated ions can

provide a significant drive for $n_{\phi} = 0$ VDOM when ICRF resonance layers are placed on the high field side of a tokamak. A key factor in this case is that, owing to pitch-angle scattering, the width of distribution function in the Λ direction implies that there is a fraction of resonating energetic ions dispersed into the passing region on flux surfaces that intersect the midplane close to the ICRF resonance radius $\omega_{\rm IC} = \omega_{\rm CI}(R_{\rm IC})$. For moderate instability frequencies, the passing ions contribute little to the damping of the $n_\phi=0$ mode, leaving the drive by energetic ions with $\Lambda > \Lambda_{IC}$ largely uncompensated. On the other hand, for on-axis resonances, a finite drive only occurs at high instability frequencies and sufficiently narrow pitch angle distributions of the ICRF accelerated ions. This implies unrealistically high energies of the ions that are resonating with the mode, and thus a very low fraction of the energetic ions is being effectively involved. A more realistic assessment of such on-axis ICRF resonances requires a proper treatment of finite orbit width effects, which is beyond the scope of this initial study. Nevertheless, our current assessment indicates that the drive would be rather weak for on axis resonances.

The results of the simulations where sawtooth crashes are applied show that it is indeed possible to create a region of energy below \mathcal{E}_{crit} with a positive slope of the distribution function in the energy direction. However, the distribution function stays energy inverted for a short period of time only, of the order of a few tens of milliseconds, mainly because the ICRF heating is a diffusive process in phase space. Furthermore, for sawtooth redistribution to be effective in creating locally energy inverted distribution functions, the ICRF resonance layer must be close the magnetic axis (well inside the q=1surface). The simulations show that in the region where the energy distributions is locally inverted, the damping due to ICRF accelerated ions with $\Lambda < \Lambda_{IC}$ is very strong. For this reason, the appearance of a region with an energy-inverted, bump-on-tail-like distribution following a simulated sawtooth crash was found to be insufficient to drive $n_{\phi} = 0$ VDOMs in the tested cases.

It should, however, be noted that sawtooth redistribution of other types of fast ion populations could contribute to the drive of vertical $n_\phi=0$ oscillatory modes. For example, in the case of fusion-born alpha particles, one would expect that positive values of $\partial f_0/\partial \mathcal{E}$ will play a more dominant role than the anisotropy represented by the $\partial f_0/\partial \Lambda$ term in equation (9) following a sawtooth redistribution (even if there would be some anisotropy in the post crash distribution since the trapped high energy ions are less affected by the redistribution than circulating ones). Furthermore, as mentioned in the introduction, there are other mechanisms that can create regions in phase space with pure bump on tail features, especially because of particle sources [15, 17] modulated on time scales that are shorter than the sawtooth period, which have the potential to drive $n_\phi=0$ modes.

As mentioned in the introduction, there are features of the presented analysis that should be relevant also to other $n_{\phi}=0$ modes. In particular, any drive due to the anisotropy of distribution functions of ICRF heated ions is expected to be more effective for high field side ICRF resonances than other locations. Furthermore, the local 'bump on tail' regions found in the simulations of the distribution functions following a sawtooth crash should be too weak to drive to $n_{\phi}=0$ modes in general.

While this exploratory assessment of the drive of vertical $n_{\phi}=0$ VDOMs by ICRF accelerated ions provides insight into features that are key for its effectiveness, it is clear that a more quantitative analysis would require taking finite orbit width effects into account. This is, however, quite a formidable task since there are few available codes that could do this efficiently. As an intermediate step, one may perhaps consider developing a simplified modelling of the distribution function including finite orbit width effects.

Acknowledgment

Fruitful discussions with Dr Tommaso Barberis (Princeton Plasma Physics Laboratory) are gratefully acknowledged.

Appendix A. Linear theory for the drive of $\mathbf{n}_\phi=\mathbf{0}$ modes

In order to derive the growth rate for $n_{\phi}=0$ modes driven by fast ions, we need to evaluate the change in energy content of the energetic ions in the presence of a perturbation. In the linear phase of an instability, the time derivative of the energy content can be obtained in different ways, see for instance [21, 23]. Here we follow more closely the latter, obtaining the time derivative of the fast ion energy content by evaluating the energy moment of a quasi-linear operator for the instability wave-particle interaction. The formulation of the quasi-linear operator for the orbit averaged distribution function f_0 presented in [21] use action angle variables $(\vec{J}, \vec{\theta})$

$$Q_{\text{inst}}(f_0) = \frac{\partial}{\partial J^i} \left[\bar{D}_{\text{inst}}^{ij} \frac{\partial f_0}{\partial J^j} \right]$$
 (A.1)

where the orbit averaged distribution function is defined by

$$f_0\left(\vec{J}\right) = \frac{1}{\left(2\pi\right)^2} \int f d^3\theta \tag{A.2}$$

and $\bar{D}_{\text{inst}}^{ij}$ tensor are given by,

$$\bar{D}_{\text{inst}}^{ij} = \pi \sum_{\vec{n}} \left| \tilde{H}_1 \left(\vec{J}, \vec{n}, \omega \right) \right|^2 \delta \left(\omega - \vec{n} \cdot \vec{\Omega} \right) n^i n^j$$
 (A.3)

Here $J^1 = m\mu/Ze$ is the normalised magnetic moment, where $\mu = mv_\perp^2/2B$ is the magnetic moment, J^2 has a complicated expression and it is not needed in what follows, $J^3 = p_\phi$ is the canonical toroidal angular momentum. Roughly speaking, the first angle θ^1 describes the position of the particle in the Larmor rotation, θ^2 the position along the guiding-centre orbit, and θ^3 the bounce averaged toroidal position of a particle; these angles evolve linearly in time with frequencies,

$$\dot{\theta}^i = \frac{\partial H_0}{\partial J^i} = \Omega^i, \tag{A.4}$$

where H_0 is the unperturbed Hamiltonian of the particle motion, Ω^1 is the orbit averaged Larmor frequency, $\Omega^2 = \omega_b$ is bounce frequency and Ω^3 the toroidal precession frequency of a particle (to lighten the notation, we do not use the subscript '0' for the instability angular frequency in this appendix). Finally, the Fourier transformed perturbed Hamiltonian, $\tilde{H}_1(\vec{J}, \vec{n}, \omega)$ is formally given by,

$$\tilde{H}_{1}(\vec{J}, \vec{n}, \omega) = \int H_{1}(\vec{J}, \vec{\theta}, \omega) e^{(-i\vec{n}\cdot\vec{\theta})} \frac{d^{3}\theta}{(2\pi)^{3}}.$$
 (A.5)

The perturbed Hamiltonian can be written as,

$$\frac{\mathrm{d}H_{1}\left(\vec{J},\vec{\theta},t\right)}{\mathrm{d}t} = Ze\vec{v}\cdot\vec{E_{1}} = Ze\left(\vec{v}_{\parallel} + \vec{v}_{d} + \vec{v}_{\perp,L}\right)\cdot\vec{E_{1}} \quad (A.6)$$

Where \vec{E}_1 is the perturbed electric field, $\vec{v}_{\perp,L}$ is the velocity associated with the Larmor rotation and \vec{v}_D is the drift velocity,

$$\vec{v}_{\rm D} = \frac{1}{\omega_c} \vec{b} \times \left(v_{\parallel}^2 \vec{\kappa} + \frac{1}{2} v_{\perp}^2 \nabla l n B \right) \tag{A.7}$$

Because we are here interested in modes with frequencies much lower than the cyclotron frequency of the energetic ions and $n_{\phi}=0$ modes, i.e. the perturbed Hamiltonian has no toroidal dependence, the resonance condition dictates that we only need to evaluate $\tilde{H_1}$ for $n_1=0$ and $n_3=n_{\phi}=0$. Denoting $n_2=p$ we find for this Fourier component,

$$\begin{split} \tilde{H_1}\left(\vec{J},p,\omega\right) &= \frac{i}{\omega} \int_0^{2\pi} \langle H_1 \rangle \mathrm{e}^{(-\mathrm{i}p\omega_b\tau)} \frac{\mathrm{d}\theta^2}{(2\pi)} \\ &= \frac{i}{\omega\tau_b} \int_0^{\tau_b} \langle H_1 \rangle \mathrm{e}^{(-\mathrm{i}p\omega_b\tau)} \mathrm{d}\tau \end{split} \tag{A.8}$$

with

$$\langle H_1 \rangle = \frac{1}{2\pi} \int_0^{2\pi} H_1 d\theta^1 = \left[Ze \left(\vec{v}_{\parallel} + \vec{v}_d \right) \cdot \vec{E}_1 + \mu \frac{\partial B_{1,\parallel}}{\partial t} \right]$$
(A.9)

where $B_{1,\parallel}$ is the perturbed magnetic field in the direction of the equilibrium magnetic field. Following [23] we consider an MHD perturbation, i.e. one that satisfies the constraint,

$$\vec{B}_1 = \nabla \times \left(\vec{\xi}_{\perp} \times \vec{B} \right) \tag{A.10}$$

where $\vec{\xi}_{\perp}$ is identified as the displacement of a field line. This implies a gauge with a perturbed vector potential perpendicular to the equilibrium magnetic field,

$$\vec{A}_1 = \vec{\xi}_\perp \times \vec{B} \tag{A.11}$$

Like in [23] we assume that the perturbed electric potential, ϕ_1 , is zero and therefore $E_{1,\parallel}=0$. Thus, we find,

$$\begin{split} \widetilde{H_{1}}\left(\vec{J},p,\omega\right) \\ &= -\frac{1}{\tau_{b}} \int_{0}^{\tau_{b}} \left[ZeB\vec{v}_{d} \cdot \left(\vec{\xi}_{\perp} \times \vec{b}\right) - \mu B_{1\parallel} \right] e^{(-ip\omega_{b}\tau)} d\tau \\ &= \frac{1}{\tau_{b}} \int_{0}^{\tau_{b}} \left[\vec{\xi}_{\perp} \cdot \left(mv_{\parallel}^{2} \vec{\kappa} + \mu \nabla B \right) + \mu B_{1\parallel} \right] e^{(-ip\omega_{b}\tau)} d\tau \end{split}$$
(A.12)

Returning to the diffusion tensor components, with $n_1=0$ and $n_3=0$, the only non-zero component of the diffusion tensor is then $D^{I_2J_2}$ (i.e. D^{22} in the notation used in equation (A.1)). However, in order to take the energy moment of the quasi-linear operator it is convenient to change from the actions \vec{J} to the set of invariants $\vec{I}=(\mathcal{E},\Lambda=\mu B_0/\mathcal{E},P_\phi)$, where $I^1=\mathcal{E}$ is the kinetic energy. In addition, a variable σ which takes the value $\sigma=v_\parallel/|v_\parallel|$ evaluated at the outer crossing of the mid-plane by a particle orbit (in the standard limit to separate between co and counter passing ions). For the transformation of the components of the diffusion tensor into the new coordinates we now only need $\partial \mathcal{E}/\partial J^2=\Omega^2$ and $\partial \Lambda/\partial J^2=-\Lambda\Omega^2/\mathcal{E}$ (where we have used the fact that \mathcal{E} is the unperturbed Hamiltonian of the particle movement). The quasi-linear operator now takes the form,

$$Q_{\text{Inst}}^{N=0}(f_0) = \sum_{\sigma} \frac{1}{\sqrt{g}} \frac{\partial}{\partial \mathcal{E}} \left[\sqrt{g} \left(D^{\mathcal{E}\mathcal{E}} \frac{\partial f_0}{\partial \mathcal{E}} + D^{\mathcal{E}\Lambda} \frac{\partial f_0}{\partial \Lambda} \right) \right] + \sum_{\sigma} \frac{1}{\sqrt{g}} \frac{\partial}{\partial \Lambda} \left[\sqrt{g} \left(D^{\Lambda\Lambda} \frac{\partial f_0}{\partial \Lambda} + D^{\Lambda\mathcal{E}} \frac{\partial f_0}{\partial \Lambda} \right) \right]$$
(A.13)

where the Jacobian is given by,

$$\sqrt{g} = \left| \frac{\partial \left(\vec{J}, \vec{\theta} \right)}{\partial \left(\vec{I}, \vec{\theta} \right)} \right| = \left| \frac{\partial \vec{J}}{\partial \vec{I}} \right| = \frac{\mathcal{E}}{ZeB_0 m^2 \omega_b}$$
 (A.14)

and,

$$\begin{split} D^{\mathcal{E}\mathcal{E}} &= \bar{D}^{J_2 J_2} \frac{\partial \mathcal{E}}{\partial J^2} \frac{\partial \mathcal{E}}{\partial J^2} = \omega^2 D_0 \\ D^{\mathcal{E}\Lambda} &= D^{\Lambda \mathcal{E}} = \bar{D}^{22} \frac{\partial \mathcal{E}}{\partial J^2} \frac{\partial \Lambda}{\partial J^2} = -\omega^2 \frac{\Lambda}{E} D_0 \\ D^{\Lambda\Lambda} &= \bar{D}^{22} \frac{\partial \Lambda}{\partial J^2} \frac{\partial \Lambda}{\partial J^2} = \left(\omega \frac{\Lambda}{\mathcal{E}}\right)^2 D_0 \end{split} \tag{A.15}$$

with,

$$D_0 = \pi \sum_{p} \left| \tilde{H}_1 \left(\vec{I}, p, \omega \right) \right|^2 \delta \left(\omega - p \omega_b \right)$$
 (A.16)

Note that by virtue of the resonance delta function, we have replaced $p\omega_b$ with ω . The energy moment of the this quasilinear operator now gives us the time derivative of the energy content of the energetic ion distribution in the liner phase, i.e.

$$\frac{\mathrm{d}W_{h}}{\mathrm{d}t} = \int \mathcal{E}Q_{\mathrm{inst}}^{N=0}(f_{0})\sqrt{g}\mathrm{d}\mathcal{E}\mathrm{d}\Lambda\mathrm{d}P_{\phi}\mathrm{d}^{3}\theta$$

$$= -(8\pi)^{3}\omega^{2}\sum_{\sigma}\int\sqrt{g}\omega^{2}D_{0}\left(\frac{\partial}{\partial\mathcal{E}} - \frac{\Lambda}{\mathcal{E}}\frac{\partial}{\partial\lambda}\right)f_{0}\mathrm{d}\mathcal{E}\mathrm{d}\Lambda\mathrm{d}P_{\phi}.$$
(A.17)

For a given instability wave frequency ω , the resonance condition determines a resonant energy \mathcal{E}_p^* as a function of p, Λ and P_{ϕ} , defined by $\omega = p\omega_b(\mathcal{E}_p^*, \Lambda, P_{\phi})$. We can eliminate the delta function in D_0 by integrating over energy to arrive at,

$$\frac{\mathrm{d}W_{h}}{\mathrm{d}t} = -8\pi^{4}\omega^{2} \sum_{\sigma} \int$$

$$\times \left[\sqrt{g} \sum_{p} \left| \tilde{H}_{1} \right|^{2} \left(p \frac{\partial \omega_{b}}{\partial \mathcal{E}} \right)^{-1} \left(\frac{\partial f_{0}}{\partial \mathcal{E}} - \frac{\Lambda}{\mathcal{E}} \frac{\partial f_{0}}{\partial \lambda} \right) \right]_{\mathcal{E} = \mathcal{E}_{p}^{*}} \mathrm{d}\Lambda \mathrm{d}P_{\phi}.$$
(A.18)

Using the definition of the variable λ_h in the main text we find,

$$\lambda_{h} = -\frac{8\pi^{4}}{W_{\text{inst}}} \omega \sum_{\sigma} \int \left[\sqrt{g} \sum_{p} \left| \tilde{H}_{1} \right|^{2} \left(p \frac{\partial \omega_{b}}{\partial \mathcal{E}} \right)^{-1} \left(\frac{\partial f_{0}}{\partial \mathcal{E}} - \frac{\Lambda}{\mathcal{E}} \frac{\partial f_{0}}{\partial \lambda} \right) \right]_{\mathcal{E} = \mathcal{E}_{p}^{*}} d\Lambda dP_{\phi}$$
(A.19)

We now turn to the thin banana width limit in which case $\mathrm{d}P_\psi \to Z \mathrm{ed}\psi$. Furthermore, we introduce $\rho = \sqrt{\psi/\psi_a}$ as flux surface coordinate, where we have defined ψ to be zero on the magnetic axis and ψ_a is the ψ at the plasma boundary. Following [14], we introduce $h_{\omega_b}(\Lambda,r) = \omega_b R_0 q/v$ and take $W_{\mathrm{inst}} = V \rho_c \omega^2 \xi^2/2$, where V is the plasma volume and ρ_c is

the core mass density. The expression for λ_h can then be cast in the form,

$$\begin{split} \lambda_h &= \frac{16\sqrt{2}\pi^4 R_0 q \psi_a}{V \rho_c \omega^2 \xi^2 B_0 m^{3/2}} \sum_{\sigma} \int \\ &\times \left[\sum_{p} \frac{\left| \tilde{H_1} \right|^2}{h_{\omega_b}} \mathcal{E}^{3/2} \left(\frac{\partial f_0}{\partial \mathcal{E}} - \frac{\Lambda}{\mathcal{E}} \frac{\partial f_0}{\partial \lambda} \right) \right]_{\mathcal{E} = \mathcal{E}^*} \rho \mathrm{d}\rho \mathrm{d}\Lambda \ \, (\mathrm{A.20}) \end{split}$$

where,
$$\sqrt{2\mathcal{E}_p^*/m}=\omega_0R_0q/[ph_{\omega_b}(\Lambda,\rho)]$$
.

At this point it is important to note that in order to assess the potential for instability, the whole energy functional must be minimised. As discussed in detail in [23], this implies minimising $B_{1\parallel}$. It is shown in [22, 23] that with an appropriate choice of $\vec{\xi}$, $B_{1\parallel}$ is of order $\mathcal{O}(\epsilon \xi/R)$. Hence, to leading order we can neglect it in the expression for λ_h above. Furthermore, in order to establish contact with [14], we now assume a low β plasma and neglect the distinction between $\vec{\kappa}$ and $B^{-1}\nabla B$, leading to,

$$\begin{split} \tilde{H_1}\left(\vec{J}, p, \omega\right) &= \frac{1}{\tau_b} \int_0^{\tau_b} \mathcal{E}\left(2 - \Lambda \frac{B}{B_0}\right) \vec{\xi} \cdot \vec{\kappa} \, \mathrm{e}^{(-\mathrm{i}p\omega_b\tau)} \mathrm{d}\tau \\ &\approx \frac{1}{\tau_b} \int_0^{\tau_b} \mathcal{E}\left(2 - \Lambda\right) \vec{\xi} \cdot \vec{\kappa} \, \mathrm{e}^{(-\mathrm{i}p\omega_b\tau)} \mathrm{d}\tau \quad \text{(A.21)} \end{split}$$

We now turn to $\vec{\xi} \cdot \vec{\kappa}$. As indicated in [14], $\vec{\xi}_{\perp}$ a rigid vertical shift in our case. Consequently, the curvature of B_{ϕ} does not contribute to $\vec{\xi} \cdot \vec{\kappa}$, instead $\partial B_{\theta}/\partial z$ is the key factor for $\vec{\xi} \cdot \vec{\kappa}$, and one finds,

$$\vec{\xi} \cdot \vec{\kappa} \approx \frac{\xi}{R} \frac{\partial B_{\theta}}{\partial \alpha} \hat{z} \cdot \nabla \rho$$
 (A.22)

For tokamak with circular flux surfaces, this expression is approximately given by,

$$\vec{\xi} \cdot \vec{\kappa} \approx \frac{\xi \, \epsilon^2}{q^2 r} sin(\theta) \tag{A.23}$$

Together equations (A.20)–(A.22) constitute the generalised form, taking into account the anisotropy of the distribution function, of equation (11) in [14]. It should be noted that $|\tilde{H}_1(\vec{J},p,\omega)|$ is equivalent to $|\Upsilon_p|$ in [14], and we adopt the latter notation in the main text.

Appendix B. Model of ICRF heated distribution function

The evolution of the distribution function of ions resonating with ICRF waves in a toroidal plasma can be described by a 3D orbit averaged Fokker–Planck equation [31],

$$\frac{\partial f_0}{\partial t} = \langle C(f_0) \rangle + \langle Q(f_0) \rangle \tag{B.1}$$

where $\langle C(f_0) \rangle$ i the orbit averaged collision operator and $\langle Q(f_0) \rangle$ a quasi-linear operator representing the effect of the wave particle interaction on the distribution function.

The orbit averaged distribution function, f_0 , is a function of three invariants of the unperturbed particle motion, e.g. the kinetic energy, \mathcal{E} , a generalised pitch angle variable, $\Lambda=\mu B_0/\mathcal{E}=(1-\xi^2)B_0/B$ and the toroidal angular momentum $P_\phi=mRv_\parallel B_\theta/B+Ze\psi$, where B_0 is the magnetic field on the magnetic axis, ψ is the poloidal flux function (poloidal flux over 2π), Z is the charge number of the resonating species The quasi-linear description of the wave particle interaction is valid provided the relative phase between the waves and the Larmor motion of the resonating ions is sufficiently randomised between successive transits of an orbit [32], which is assumed to be the case.

Resolving the full 3D orbit averaged Fokker–Planck equation is cumbersome and costly numerically, and it is not suitable for the current exploratory study. For this reason, we seek to simplify the equation. The first step in the simplification procedure is to neglect spatial transport of the resonating ions (either by neoclassical effects or by wave-induced transport). Furthermore, we adopt the small banana width limit (i.e. $P_{\phi} \approx Ze\psi$). In this case the distribution function on a flux surface is just a function of $f_0 = f_0(\mathcal{E}, \Lambda)$ and the operator derived in [31] reduces to,

$$\begin{split} \langle \mathcal{Q}(f_0) \rangle &= \frac{1}{\sqrt{g}} \frac{\partial}{\partial \mathcal{E}} \left[\sqrt{g} D^{\mathcal{E}\mathcal{E}} \frac{\partial f_0}{\partial \mathcal{E}} \right] + \frac{1}{\sqrt{g}} \frac{\partial}{\partial \mathcal{E}} \left[\sqrt{g} D^{\mathcal{E}\Lambda} \frac{\partial f_0}{\partial \Lambda} \right] \\ &+ \frac{1}{\sqrt{g}} \frac{\partial}{\partial \Lambda} \left[\sqrt{g} D^{\Lambda \mathcal{E}} \frac{\partial f_0}{\partial \mathcal{E}} \right] + \frac{1}{\sqrt{g}} \frac{\partial}{\partial \Lambda} \left[\sqrt{g} D^{\Lambda \Lambda} \frac{\partial f_0}{\partial \Lambda} \right] \end{split}$$

where $\sqrt{g} = \mathcal{E}/(m^2 Ze B_0 \omega_b)$,

$$egin{aligned} D^{\mathcal{E}\mathcal{E}} &= \omega_{ ext{IC}}^2 D_0 \ D^{W\Lambda} &= D^{\Lambda\mathcal{E}} &= rac{\omega_{ ext{IC}} \left(n \omega_{ ext{ci},0} - \Lambda \omega_{ ext{IC}}
ight)}{\mathcal{E}} D_0 \ D^{\Lambda\Lambda} &= \left(rac{n \omega_{ ext{ci},0} - \Lambda \omega_{ ext{IC}}}{\mathcal{E}}
ight)^2 D_0 \end{aligned}$$

 $\omega_{ci,0}$ is the ion cyclotron frequebcy on the magnetic axis and,

$$\begin{split} D_0 &= \frac{1}{2\tau_b} \left(\frac{Ze}{\omega_{\rm IC}} \right)^2 \left| \oint_{\rm orbit} \right. \\ &\times \nu_{\perp} \left[E_+ J_{n-1} \left(\frac{k_{\perp} \nu_{\perp}}{\omega_c} \right) + E_- J_{n+1} \left(\frac{k_{\perp} \nu_{\perp}}{\omega_c} \right) \right] \mathrm{e}^{\mathrm{i} \, \phi} \right|^2 \mathrm{d}t \\ &\frac{\mathrm{d}\phi}{\mathrm{d}t} = n \omega_c - \omega_{\rm IC} + k_{\parallel} \nu_{\parallel}. \end{split}$$

In the PION code D_0 is approximated by,

$$D_0 = E_{\text{norm}}^2 \left| J_{n-1} \left(\frac{k_{\perp} v_{\perp}}{\omega_c} \right) + \frac{E_-}{E_+} J_{n+1} \left(\frac{k_{\perp} v_{\perp}}{\omega_c} \right) \right|_R^2$$

where R stands for the quantity evaluated at a local resonance point and the normalising factor, E_{norm}^2 is adjusted such that the flux surface averaged power density is consistent with that obtained from the wave propagation model.

We now define the pitch angle averaged distribution function as,

$$F(\mathcal{E}) = \int f_0 J d\Lambda \tag{B.2}$$

where,

$$J = \frac{\pi \, v \tau_b}{2 \frac{\mathrm{d}V}{\mathrm{d}vb} B_0}.\tag{B.3}$$

 $V(\psi)$ is the volume enclosed by a flux surface labelled by the poloidal flux ψ . This is the natural definition because if we take a velocity independent moment $y(\mathcal{E})$ of the distribution function (e.g. $y = \mathcal{E}$ to calculate the energy density of the resonating ions species) we find,

$$\langle y \rangle_{fl.s} = \lim_{\Delta \psi \to 0} \frac{\int d\mathcal{E} \int d\Lambda \int_{\psi}^{\psi + \Delta \psi} y(\mathcal{E}) f_0 \sqrt{g} 8\pi^3 Zed\psi}{\frac{dV}{d\psi} \Delta \psi}$$

$$= 4\pi \int y(\mathcal{E}) F(\mathcal{E}) \frac{\sqrt{2\mathcal{E}}}{m^{3/2}} d\mathcal{E}$$

$$= 4\pi \int y(v) F(v) v^2 dv.$$
(B.4)

(The $8\pi^3$ stems from the integration of the three action angles employed in e.g. [31])

We now make the ansatz that the distribution function can be written as,

$$f_0(v, \Lambda) = F(\mathcal{E}) h(\mathcal{E}, \Lambda)$$
 (B.5)

where the function h is normalised such that,

$$\int_{0}^{B_0/B_{\min}} Jh(\mathcal{E}, \Lambda) d\Lambda = 1.$$
 (B.6)

The PION code solves for the pitch angle averaged distribution function,

$$\frac{\partial F}{\partial t} = \langle \langle C(F) \rangle \rangle_{\Lambda} + \langle \langle Q(F) \rangle \rangle_{\Lambda}$$
 (B.7)

where

$$\langle (\ldots) \rangle_{\Lambda} = \int_{0}^{B_0/B_{\min}} (\ldots) J d\Lambda$$
 (B.8)

For the function $h(\mathcal{E},\Lambda)$, we change the coordinate Λ to the pitch angle where the orbit crosses the mid-plane on the low field side, $\xi=\pm\sqrt{1-\Lambda B_{\rm m}/B_0}$, where $B_{\rm m}$ is the magnetic field at the mid-plane. Furthermore, consider the point on the flux surface where the poloidal angle is given by, $\omega_{\rm IC}=n\omega_c(\rho,\theta_R)$, and denote the local pitch angle at $\theta=\theta_R$ by $\mu=\nu_{\parallel,R}/\nu$. Thus, we have $\mu=\pm\sqrt{[1-(1-\xi^2)B_m/B_R]}$ and the local distribution function at $\theta=\theta_R$ is given by,

$$f_0(\mathcal{E}, \mu, \theta_R) = f_0(\nu, \xi(\mu, \theta_R)). \tag{B.9}$$

In order to obtain an h representing the characteristic 'rabbit ear' shape of the level surfaces of ICRF heated distribution functions, see [28], we make the ansatz,

$$h(\mathcal{E},\xi) = K_{\text{norm}} \left[e^{\left(\frac{\xi - \xi_R}{\sigma(\mathcal{E})}\right)^2} + e^{\left(\frac{\xi + \xi_R}{\sigma(\mathcal{E})}\right)^2} \right]$$
 (B.10)

with the normalisation constant, K_{norm} , determined from equation (B.6), and $\xi_R = \sqrt{1 - B_m/B_R}$. In order to determine the width, σ , the μ^2 moment is calculated at the point $\theta = \theta_R$ and as an approximation σ is adjusted such that this momenet matches the $\mu_{\text{eff}}(\mathcal{E})$ used in PION to estimate the parallel energy content of the resonating ions,

$$\mu_{\text{eff}}^2(\mathcal{E}) \approx \int \mu^2 h[\mathcal{E}, \xi(\mu, \theta_R)] d\mu,$$
 (B.11)

with,

$$\mu_{\text{eff}}^{2}(\mathcal{E}) = \frac{1}{3} \frac{1 + \frac{\mathcal{E}}{\mathcal{E}_{*}}}{1 + \frac{\mathcal{E}}{\mathcal{E}_{*}} + \left(\frac{\mathcal{E}}{\mathcal{E}_{*}}\right)^{2}}$$
(B.12)

and $\mathcal{E}_* = \mathcal{E}_{\gamma}/4$, where \mathcal{E}_{γ} is the characteristic velocity associated with pitch angle scattering [29]. The factor 1/4 was obtained by comparison with simulations by the 2D bounce averaged Fokker–Planck code BAFIC [33].

This model has been implemented in an updated version of the PION code, which calculates σ and K_{norm} from which the 2D distribution function can then be reconstructed.

Appendix C. Heuristic model of the high energy distribution function

As discussed in section 4, the distribution of ICRF accelerated ion becomes very narrow around the value of Λ corresponding to the turning point of trapped ions just reaching the cold resonance defined by $\omega_{\rm IC} = n\omega_c(B_{\rm Res})$. We use this fact in order to construct a heuristic, or mock-up model, of the high energy distribution suitable for analytic work. Taking inspiration from appendix B we start from the following approximate form for the distribution function,

$$f_{0}\left(v_{\perp R}, v_{\parallel R}, r\right) \approx C_{0} \sqrt{\frac{m}{2\pi T_{0}}} \exp\left(-\frac{mv_{\perp R}^{2}}{2T_{\text{tail}}}\right) \exp\left(-\frac{m\left(v_{\parallel R} - \sigma\epsilon v\right)^{2}}{2T_{0}}\right) \tag{C.1}$$

where $v_{\perp R}$ and $v_{\parallel R}$ are the perpendicular and parallel velocities of accelerated high energy ions measured at $\omega_{\rm IC} = n\omega_c(R_{\rm IC})$, $\sigma = v_{\parallel R}/|v_{\parallel R}|$ and ϵv a small velocity introduced to ensure that the average turning point of resonant ions is just beyond the cold resonance (note: here ϵ is just a small parameter and not the inverse aspect ratio). We can now express $v_{\perp R}$ and $v_{\parallel R}$ in terms of v and Λ ,

$$v_{\perp R}^2 = v^2 \frac{\Lambda}{\Lambda_{1C}} \tag{C.2}$$

$$v_{\parallel R}^2 = \sigma v \sqrt{1 - \frac{\Lambda}{\Lambda_{\rm IC}}} \tag{C.3}$$

where $\Lambda_{\text{Res}} = \frac{B_0}{B_R}$. We now take the limit $T_0 \to 0$, to obtain,

$$f_0(\mathcal{E}, \Lambda, \rho) \approx C_0 \exp\left(-\frac{\mathcal{E}}{T_{\text{tail}}} \frac{\Lambda}{\Lambda_{\text{IC}}}\right) \delta \left[\sigma v \left(\sqrt{1 - \frac{\Lambda}{\Lambda_{\text{IC}}}} - \epsilon\right)\right].$$
(C.4)

In the main text, we employ integrals over Λ of the distribution function and therefore transform the delta function yielding,

$$f_0\left(\mathcal{E}, \Lambda, r\right) \approx C_0 \frac{2\epsilon}{\nu} \exp\left(-\frac{\mathcal{E}}{T_{\text{tail}}} \frac{\Lambda}{\Lambda_{\text{IC}}}\right) \delta\left[\Lambda - \Lambda_{\text{IC}} \left(1 - \epsilon^2\right)\right].$$
(C.5)

In order to fix C_0 we take the density moment of the distribution, which should yield the density of the energetic ions, n_f . Using the results in appendix B, we have,

$$n_{\text{res}}(r) = \frac{\sqrt{2}\pi}{m^{3/2}} \int f_0(\mathcal{E}, \Lambda, r) \frac{\sqrt{\mathcal{E}}}{h_{\omega_b}(\Lambda)} d\mathcal{E}d\Lambda$$

$$= \frac{2\pi C_0 \epsilon}{m h_{\omega_b} \left[\Lambda_{IC} (1 - \epsilon^2)\right]} \int_0^\infty \exp\left(-\frac{\mathcal{E}}{T_{\text{tail}}} \left(1 - \epsilon^2\right)\right) d\mathcal{E}.$$
(C.6)

Thus, $C_0\epsilon = n_{\rm res}h_{\omega_b}[\Lambda_{\rm IC}(1-\epsilon^2]/[2\pi T_{\rm tail}(1-\epsilon^2)]$ and finally in the limit $\epsilon \to 0$ we obtain,

$$f_0\left(\mathcal{E}, \Lambda, r\right) pprox rac{n_f m^{3/2} h_{\omega_b}\left(\Lambda_{
m IC}
ight)}{2^{3/2} \pi \, T_{
m tail}} rac{\exp\left(-rac{\mathcal{E}}{T_{
m tail}}
ight)}{\sqrt{\mathcal{E}}} \delta\left(\Lambda - \Lambda_{
m IC}
ight).$$
 (C.7)

The key point to observe here is the $1/\sqrt{\mathcal{E}} \sim 1/v$ dependence, which stems from the fact that, loosely speaking, when the distribution is very narrow in Λ effectively one degree of freedom has been removed from the particle motion. Intuitively $v \to v_{\perp}$ and therefore $(...)(1/v)v^2dv \to (...)v_{\perp}dv_{\perp}$. Of course, it must be emphasised that the above model distribution is only valid in the high energy range and cannot be extrapolated to thermal energies.

As is shown in section 5, the $1/\sqrt{\mathcal{E}}$ dependence does have an influence on the threshold for flux surface to provide a positive contribution to the $n_{\phi}=0$ instability that cannot always be neglected.

In the limit of very strong tail formation, the tail temperature is related to the absorbed ICRF power density and the ion-electron collisional slowing down time by,

$$n_{\text{res}} T_{\text{tail}}(r) \approx p_{\text{ICRF}}(r) t_s / 2.$$
 (C.8)

ORCID iDs

L.-G. Eriksson © 0009-0004-1375-9929 F. Porcelli © 0000-0002-3625-6417

References

- [1] Start D.F.H. et al 1999 Nucl. Fusion 39 321
- [2] Bergeaud V., Eriksson L.G. and Start D. 2000 Nucl. Fusion 40 35
- [3] Stix T. 1992 Waves in Plasmas (Springer)
- [4] Chen L. and Zonca F. 2016 Rev. Mod. Phys. 88 015008
- [5] Sharapov S. 2021 Energetic Particles in Tokamak Plasmas (CRC Press)
- [6] Lister J.B. et al 1990 Nucl. Fusion 30 2349
- [7] Hutchinson I. 1989 Nucl. Fusion 29 2107
- [8] Winsor N., Johnson J.L. and Dawson J.M. 1968 Phys. Fluids 11 2448–50
- [9] Villard L. and Vaclavik J. 1997 Nucl. Fusion 37 351
- [10] Barberis T., Yolbarsop A. and Porcelli F. 2022 J. Plasma Phys. 88 905880511
- [11] Fu G.Y. 2008 Phys. Rev. Lett. 101 185002
- [12] Berk H. 2006 Nucl. Fusion 46 S888
- [13] Oliver H.J.C., Sharapov S.E., Breizman B.N. and Zheng L.-J. 2017 Phys. Plasmas 24 122505
- [14] Barberis T. et al 2022 Nucl. Fusion 62 064002
- [15] Van Zeeland M. et al 2021 Nucl. Fusion 61 066028
- [16] Barberis T. et al 2024 Nucl. Fusion 64 126064
- [17] Barberis T. and Porcelli F. 2024 Plasma Phys. Control. Fusion 66 075007
- [18] Hellsen C., Mantsinen M., Conroy S., Ericsson G., Eriksson J., Kiptily V.G. and Nabais F. 2018 Nucl. Fusion 58 056021
- [19] Kolesnichenko Y.I., Lutsenko V.V., White R.B. and Yakovenko Y.V. 2000 Nucl. Fusion 40 1325
- [20] Jaulmes F., Westerhof E. and de Blank H.J. 2014 Nucl. Fusion 54 104013
- [21] Kaufman A.N. 1972 Phys. Fluids 15 1063
- [22] Porcelli F. et al 1988 Phys. Fluids 31 1630
- [23] Porcelli F., Stankiewicz R., Kerner W. and Berk H.L. 1994 Phys. Plasmas 1 470
- [24] Eriksson L.-G., Hellsten T. and Willen U. 1993 Nucl. Fusion 33 1037
- [25] Hellsten T. and Villard L. 1998 Nucl. Fusion 28 285
- [26] Eriksson L.-G. and Hellsten T. 1995 *Phys. Scr.* **52** 70
- [27] Eriksson L.-G., Mantsinen M.J., Hellsten T. and Carlsson J. 1999 Phys. Plasmas 6 513
- [28] Kerbel G. and McCoy M. 1985 Phys. Fluids 28 3629
- [29] Stix T. 1975 Nucl. Fusion 15 737
- [30] Anderson D., Kolesnichenko Y., Lisak M., Wising F. and Yakovenko Y. 1994 Nucl. Fusion 34 217
- [31] Eriksson L.-G. and Helander P. 1994 *Phys. Plasmas* 1 308
- [32] Bécoulet A., Gambier D. and Samain A. 1991 *Phys. Fluids* 83 137
- [33] Anderson D., Eriksson L.-G. and Lisak M. 1987 Plasma Phys. Control. Fusion 29 891